SFRP1 modulates astrocyte-to-microglia crosstalk in acute and chronic neuroinflammation

Javier Rueda-Carrasco[1,2] , María Jesús Martin-Bermejo[1,2,†], Guadalupe Pereyra[1,2,†],
María Inés Mateo[1,2,†], Aldo Borroto[1], Frederic Brosseron[3,4] , Markus P Kummer[3,4],
Stephanie Schwartz[3,4], José P López-Atalaya[5] , Balbino Alarcon[1] , Pilar Esteve[1,2],
Michael T Heneka[3,4] & Paola Bovolenta[1,2,*]

Abstract

Neuroinflammation is a common feature of many neurodegenerative diseases. It fosters a dysfunctional neuron–microglia–astrocyte crosstalk that, in turn, maintains microglial cells in a perniciously reactive state that often enhances neuronal damage. The molecular components that mediate this critical communication are not fully explored. Here, we show that secreted frizzled-related protein 1 (SFRP1), a multifunctional regulator of cell-to-cell communication, is part of the cellular crosstalk underlying neuroinflammation. In mouse models of acute and chronic neuroinflammation, SFRP1, largely astrocyte-derived, promotes and sustains microglial activation, and thus a chronic inflammatory state. SFRP1 promotes the upregulation of components of the hypoxia-induced factor-dependent inflammatory pathway and, to a lower extent, of those downstream of the nuclear factor-kappa B. We thus propose that SFRP1 acts as an astrocyte-to-microglia amplifier of neuroinflammation, representing a potential valuable therapeutic target for counteracting the harmful effect of chronic inflammation in several neurodegenerative diseases.

Introduction

Degeneration of neurons occurs in a variety of rare and common pathological conditions of the central nervous system (CNS) including Alzheimer's disease (AD) or multiple sclerosis (MS). CNS function is supported by a robust neuron–glia crosstalk (Jha *et al*, 2019; Marinelli *et al*, 2019) so that neuronal damage is almost invariably associated with the activation of two types of glial cells: microglia and astrocytes. The prompt glial response to insults brings about an inflammatory reaction that favours tissue healing and helps restoring CNS homeostasis (Ransohoff, 2016; Escartin *et al*, 2019). However, excessive glial activation, as often occurs in neurodegeneration, is itself a cause of neuronal damage, which, in turn, establishes a state of pernicious chronic neuroinflammation (Frank-Cannon *et al*, 2009; Glass *et al*, 2010; Perry & Holmes, 2014; Escartin *et al*, 2019). Consistent with an important cellular crosstalk, glial cell dysfunction, either as a consequence of hyper- or hypofunctionality, can also be the cause of neuronal damage, rather than its consequence, strongly contributing to the progression of neurodegenerative diseases (Ransohoff, 2016; Sarlus & Heneka, 2017; Hickman *et al*, 2018; Escartin *et al*, 2019). Although this is nowadays a widely accepted idea, there is still only partial information on the molecular components that sustain a dys- or hyperfunctional state of glial cells and an abnormal glia–neuron crosstalk. Here, we have investigated whether SFRP1 may represent one of such components.

SFRP1 is a small, secreted and dispersible protein with functions that have been related to Wnt signalling (Esteve & Bovolenta, 2010) and ADAM10 activity (Esteve *et al*, 2011a), although its interaction with other factors such as RANKL (receptor activator of nuclear factor-kappa B ligand), integrins (Bovolenta *et al*, 2008) and thrombospondin-1 (Martin-Manso *et al*, 2011) has also been reported. In particular, Wnt signalling not only has been mostly implicated in moulding neurodegenerative synaptic changes (Palomer *et al*, 2019) but also contributes to neuroinflammation, although this role is still ill-defined (Aghaizu *et al*, 2020). ADAM10, a member of the A Disintegrin and Metalloprotease family of plasma membrane proteins (Saftig & Lichtenthaler, 2015), acts as an α-

1 Centro de Biología Molecular Severo Ochoa, CSIC-UAM, Madrid, Spain
2 CIBER de Enfermedades Raras (CIBERER), Madrid, Spain
3 Neurology, Universitätsklinikum Bonn, Bonn, Germany
4 German Center for Neurodegenerative Diseases (DZNE), Bonn, Germany
5 Instituto de Neurociencias, CSIC-UMH, Sant Joan d'Alacant, Spain
*Corresponding author. Tel: +34 91 1964718; E-mail: pbovolenta@cbm.csic.es
†These authors contributed equally to this work

secretase (or sheddase; Lichtenthaler *et al*, 2018) for many neuronal or glial expressed substrates, which participate in the control of microglial activation (Marinelli *et al*, 2019). These include TREM2 (triggering receptor expressed on myeloid) (Kleinberger *et al*, 2014) and CD200 and CX$_3$CL1 (Hundhausen *et al*, 2007; Wong *et al*, 2016). ADAM10 also sheds proteins involved in synaptic plasticity, such as N-cadherin or the amyloid precursor protein (APP) (Musardo *et al*, 2014; Saftig & Lichtenthaler, 2015). Consistently, genetic inactivation of *Adam10* in mice causes neuroinflammation and loss of synaptic plasticity (Prox *et al*, 2013), whereas genetic studies in humans have demonstrated a link between impaired ADAM10 activity and AD (Suh *et al*, 2013; Kunkle *et al*, 2019), in part linked to its non-amyloidogenic processing of APP (Kuhn *et al*, 2010). Supporting this possibility, we have recently shown that elevated levels of SFRP1 contribute to AD pathogenesis, acting as an endogenous negative modulator of ADAM10 (Esteve *et al*, 2019b). SFRP1 upregulation correlates with poor ADAM10-mediated processing of APP and N-cadherin, whereas neutralization of its activity prevents the appearance of AD pathological traits, including glial cell activation (Esteve *et al*, 2019b).

Sfrp1 is abundantly expressed in mammalian radial glial progenitors of the developing CNS (Campanelli *et al*, 2008; Esteve *et al*, 2011a, 2019a) but is largely downregulated in the adult brain with the exception of restricted neurogenic areas (Augustine *et al*, 2001; Zhang *et al*, 2016; Esteve *et al*, 2019a). Besides in human neurodegenerative diseases (Blalock *et al*, 2004; Esteve *et al*, 2019b; Folke *et al*, 2019; Bai *et al*, 2020; preprint: Johnson *et al*, 2021), SFRP1-upregulated expression has been reported in several other inflammatory conditions such as periodontitis, rheumatoid arthritis, uropathies or pulmonary emphysema (Esteve & Bovolenta, 2010; Claudel *et al*, 2019). An upregulation has been also observed in aged brains (Folke *et al*, 2019), in which a low-grade chronic inflammation is present (Youm *et al*, 2013). Notwithstanding, whether SFRP1 is directly involved in the modulation of neuroinflammation remains unexplored.

By addressing this issue, here we show that SFRP1 is a novel mediator of the astrocyte-to-microglia crosstalk that underlies mammalian CNS inflammation. In mice, SFRP1, largely astrocyte-derived, is sufficient to activate microglial cells and to amplify their response to distinct acute and chronic neuroinflammatory challenges, sustaining their chronic activation. From a molecular point of view, SFRP1 allows for the full expression of downstream targets of the transcription factors hypoxia-induced factors (HIFs) and, to a lesser extent, nuclear factor-kappa B (NF-κB), which are mediators of neuroinflammatory responses (Helton *et al*, 2005; Kaltschmidt & Kaltschmidt, 2009). Thus, neutralizing SFRP1 function may

represent a strategy to counteract pernicious chronic neuroinflammation that contributes to many human neurodegenerative conditions.

Results

Acute brain neuroinflammation elevates astrocyte-specific levels of SFRP1 expression

To evaluate a possible link between SFRP1 and neuroinflammation, we induced acute brain inflammation by injecting bacterial lipopolysaccharides (LPS; Wright, 1999) or control saline into the somatosensory cortex of 3-month-old *Sfrp1$^{+/\beta gal}$;CX$_3$CR1$^{+/GFP}$* mice ($n = 4$), which allow the simultaneous identification of microglial (GFP; Jung *et al*, 2000) and *Sfrp1*-producing (nuclear βgal-positive; Satoh *et al*, 2006) cells. In a separate set of experiments, we performed similar injections in wt and *Sfrp1$^{+/\beta gal}$* mice ($n = 5$). Immunofluorescence of the brains three days after injection, when inflammation is at its peak (Rivest, 2009), revealed a broader βgal immunoreactivity (reporter of *Sfrp1* expression) in LPS vs saline-treated animals (Fig 1A), largely localized in GFAP$^+$ astrocytes (Fig 1A), as also reported in demyelinating or kainic acid-induced CNS lesions (Huang *et al*, 2020; García-Velázquez & Arias, 2021). Using RNAscope, we had previously detected *Sfrp1* mRNA in some Iba$^+$ microglial cells surrounding amyloid plaques present in an AD-like mouse model (Esteve *et al*, 2019b). However, we failed to detect βgal$^+$ signal in these cells after LPS injection in neither *Sfrp1$^{+/\beta gal}$;CX$_3$CR1$^{+/GFP}$* (Fig 1A) or *Sfrp1$^{+/\beta gal}$* (Fig 1C). This observation was confirmed by RNA-seq analysis of isolated microglial cells (see the last section of the results) and likely reflects the reported heterogeneous and disease-dependent activation of microglial cell (Bachiller *et al*, 2018).

Immunodetection of SFRP1 with specific antibodies (Esteve *et al*, 2019b) confirmed an increased SFRP1 production after LPS compared with saline injections (Fig 1B). Notably, SFRP1 protein distribution in saline-injected animals was comparable to that of non-injected mouse brains (Esteve *et al*, 2019b). Consistent with the secreted and dispersible nature of SFRP1 (Mii & Taira, 2009; Esteve *et al*, 2011b), immunosignal was widely distributed in the brain parenchyma (arrows, Fig 1B) and localized to the choroid plexus (not shown) but completely absent in *Sfrp1$^{-/-}$* brains (Fig 1D), as previously reported (Esteve *et al*, 2019b). The use of a highly specific ELISA (Esteve *et al*, 2019b) further confirmed a significant increase of SFRP1 levels in extracts of small cortical tissue samples—dissected in the proximity of the injection

---

Figure 1. Astrocytes upregulate SFRP1 expression upon LPS stimulation.

A–D Confocal image analysis of cryostat sections from adult *CX$_3$CR1$^{+/GFP}$; Sfrp1$^{+/\beta gal}$* (A, B); *Sfrp1$^{+/\beta gal}$* (C) and *CX$_3$CR1$^{+/GFP}$;Sfrp1$^{-/-}$* (D) and mouse brains three days after intracortical infusion of saline or LPS. Sections were immunostained for βgal (magenta, green in C) and Iba1 (green in A; red in C) or Sfrp1 (magenta) and GFP (green, B and D), and GFAP (cyan in A, B, D, red in C). Arrowheads indicate βgal/GFAP (A) and Sfrp1/GFP co-localization (B). No Sfrp1 protein is detected in the null mice independently of the treatment (two bottom lines). Scale bar: 25 μm.

E ELISA determination of Sfrp1 levels in brain extracts from 3-month-old wt and *Sfrp1$^{-/-}$* mice. WT mice were injected either with saline or with LPS. Three days after injection, the region around the injected side (10 mm^3 cortical cube) was isolated and SFRP1 content compared with that present in similar region of non-injected or *Sfrp1$^{-/-}$* mice used as negative control ($n = 5$ mice for each group). Error bars represent standard error. Statistical significance: ns $P > 0.5$
****$P < 0.0001$; one-way ANOVA followed by the Bonferroni multiple comparisons test.
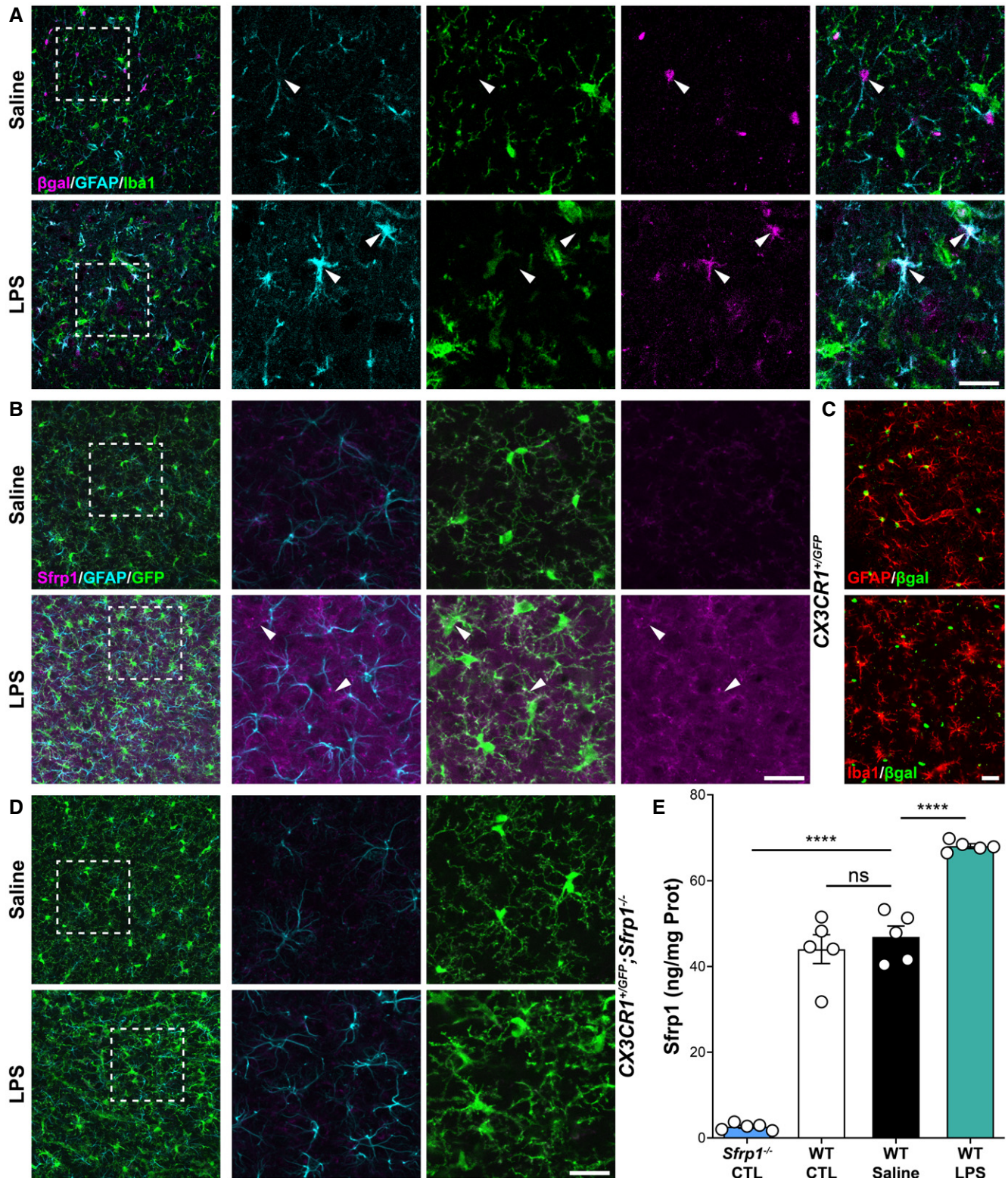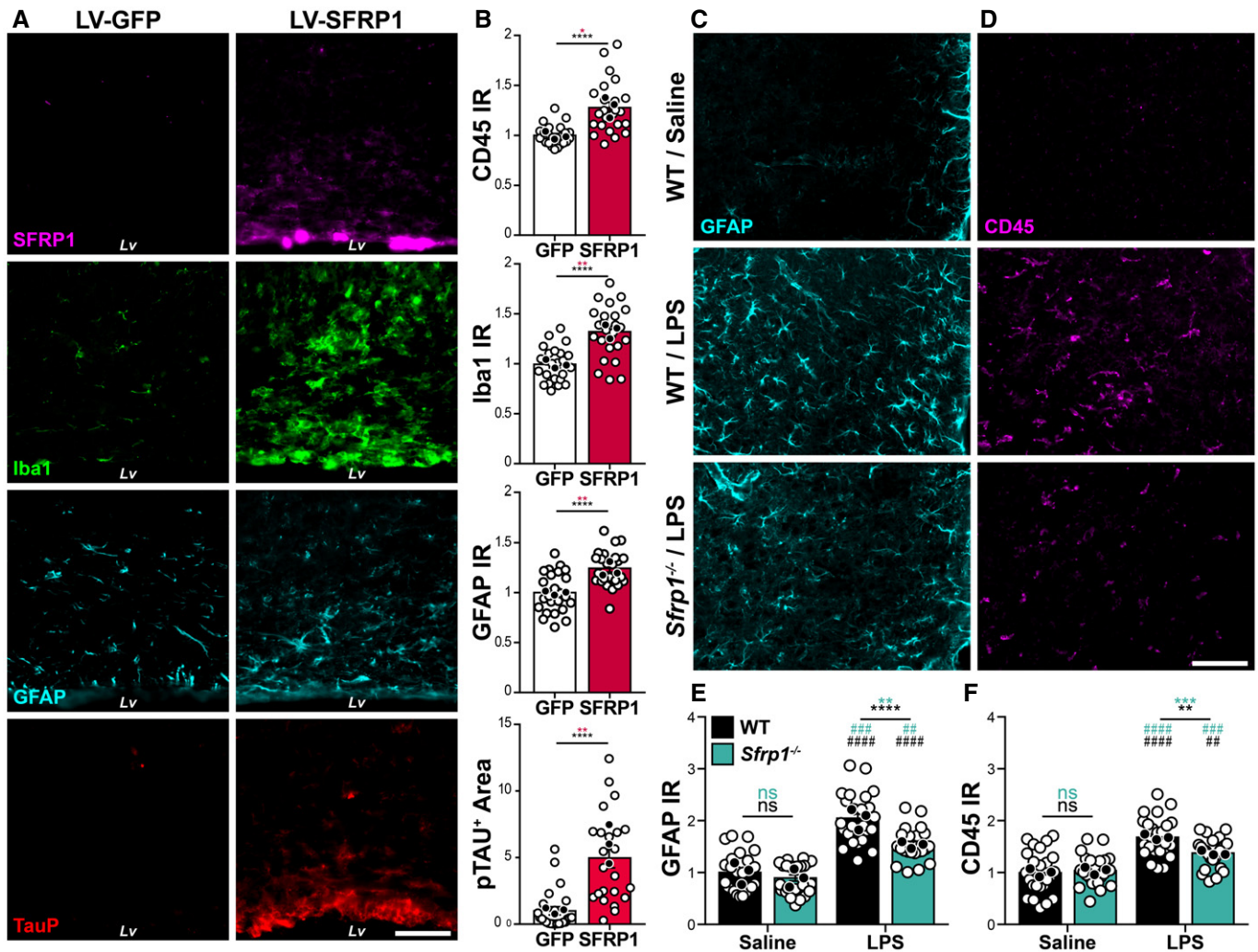
Figure 1.

site—from LPS-treated animals (Fig 1E) as compared to that present in equivalent brain regions from non-injected or saline-injected animals (Fig 1E).

These data indicate that the level of brain SFRP1 increases in response to a bacterial lipopolysaccharide and that astrocytes are likely the most abundant source of SFRP1.

***In vivo Sfrp1* gene addition is sufficient to trigger and sustain glial cell activation**

We next reasoned that if SFRP1 is indeed associated with neuroinflammation, its forced expression should be sufficient to activate glial cells. To test this possibility, we next infused lentiviral particles (LV) containing *Sfrp1*-IRES-*Gfp* or control IRES-*Gfp* into the lateral ventricle of 8- to 10-week-old wt mice (*n* = 13 per group; Figs 2 and EV1A). As expected by the injection site, GFP⁺ (used to determine

infection efficiency) LV-transduced cells included cells lining along the wall of the lateral ventricle, the choroid plexus, GFAP⁺ astrocytes and, to a lesser extent, cells of the rostral migratory stream (Fig EV1A and B). Immunohistochemistry of cortical sections 1 month after injection showed a significantly higher presence of SFRP1 protein at the infected site (Fig 2A) associated with Sox9⁺, GFAP⁺ and S100 β⁺ reactive astrocytes (Escartin *et al*, 2021) and CD45⁺, Clec7a⁺ and Iba1⁺ microglial cells as compared to LV-IRES-*Gfp* control animals (Figs 2A and B, and EV1C). Iba1

Figure 2. SFRP1 is sufficient and required to enhance glial cell activation upon LPS treatment.

A   Coronal cryostat sections of LV-IRES-*Gfp*- or LV-*Sfrp1*-IRES-*Gfp*-infected brains 1 month post-infusion immunostained for SFRP1 (magenta), Iba1 (green), GFAP (cyan) or TauP (red). Lv, lateral ventricle. Scale bar: 100 μm.

B   The graph shows the normalized level of GFAP, Iba1 and CD45 immunoreactivity (IR) and the area occupied by TauP signal (*n* = 24 acquisitions, white dots; *N* = 3 mice, black dots, for each group), normalized to LV-*IRES-Gfp*-infected brains. Error bars represent standard error. Statistical significance: *P < 0.05; **P < 0.01; ****P < 0.0001 by two-sided Student's *t*-test.

C, D   Coronal sections from wt and *Sfrp1⁻/⁻* mouse brains three days after infusion of saline or LPS immunostained for GFAP (cyan, C) or CD45 (magenta, D). The images are high-power views of the somatosensory cortex (lower power view in Fig EV1D). Scale bar: 60 μm.

E, F   The graphs show the normalized levels of immunoreactivity (IR) for GFAP (E) and CD45 (F, P = 0.006) present in cortical sections (*n* = 24 acquisitions white dots; from *N* = 3 animals, black dots, per group) from wt and *Sfrp1⁻/⁻* animals infused with saline or LPS. Bars represent standard error. Statistical significance calculated per biological replicas is indicated in green and that based on number of acquisitions in black. ** or ##P < 0.01; *** or ###P < 0.001; and **** or ####P < 0.0001 by two-way ANOVA followed by Bonferroni's multiple comparisons test. * and # indicate significance between genotypes and treatments, respectively.

immunoreactivity was accumulated around the injection site (Fig 2A and B), and many cells had a round amoeboid morphology and a significantly higher CD45 expression (Figs 2B and EV1D), characteristics of activated microglia (Heneka et al, 2014). CD45^{hi} round cells could also represent blood-borne infiltrating macrophages (Fig EV1D), although the molecular and functional difference between the two cell types is currently a matter of debate (Grassivaro et al, 2020; Honarpisheh et al, 2020). A wider distribution of hyperphosphorylated tau, which often appears as a brain response to inflammation and degeneration (Ising et al, 2019), was also detected in LV-Sfrp1-IRES-Gfp-transduced vs control brains with a significantly wider distribution (Fig 2A and B). Analysis of a different set of LV-transduced animals (n = 4) 5 months after LV delivery showed a persistent microglial activation in SFRP1- vs GFP-treated animals, with more CD45^{+} cells than those observed at 1-month post-injection (Fig EV1D). Furthermore, several CD45^{hi} round-shaped microglia/macrophages were detected in the parenchyma, especially in the proximity of transduced cells (white arrowheads in Fig EV1D).

Together, these results indicate that SFRP1 is sufficient to trigger an inflammatory response in glial cells, which persists for prolonged periods of time.

Sfrp1 is required for amplifying CNS inflammatory response

Given that SFRP1 was sufficient to induce glial cell activation, we next asked whether it was also a necessary component of the CNS inflammatory response. To this end, we took advantage of Sfrp1^{−/−} mice, in which SFRP1 protein is completely undetectable (Esteve et al, 2019b) (Fig 1B and C). These mice have a slightly shorter and thicker cortex that however does not affect their life span, reproduction rate or cognitive and motor behaviour and present no evident neuronal defects (Esteve et al, 2019a, 2019b). Furthermore, their content of astrocytes and microglial cells was undistinguishable from that of wt mice (Fig 2C–F). We thus compared the effect of intracortical LPS infusion into the brains of 3-month-old wt and Sfrp1^{−/−} mice (Fig 2C and D). In the somatosensory cortex of wt brains (Fig EV1E), LPS but not saline treatment caused the appearance of GFAP^{+} reactive astrocytes (Fig 2C) and CD45^{+} reactive microglia (Fig 2D). In contrast, Sfrp1^{−/−} littermates presented fewer and less immunopositive astrocytes and a significant reduction in CD45^{+} reactive microglia/macrophages (Fig 2C and D), further supporting that SFRP1 is relevant for the activation of both astrocytes and microglial cells. Quantitation of immunoreactivity among different genotypes and treatments confirmed no significant differences between the two saline-treated genotypes but showed a significantly lower response of Sfrp1^{−/−} mice to LPS as compared to wt (Fig 2E and F). Nevertheless, Sfrp1^{−/−} mice do not completely lose their response to LPS, given that this is significantly different from that observed in saline-injected mice (Fig 2E and F). This suggests that SFRP1 is involved in boosting inflammation.

To evaluate a possible specificity of this response, we induced experimental autoimmune encephalomyelitis (EAE) in wt and Sfrp1^{−/−} mice. This is a widely used experimental model for MS, a human inflammatory-demyelinating disease. In EAE, CNS inflammation and gliosis occur as a consequence of a strong autoimmune response against the peripheral exposure to myelin components (Constantinescu et al, 2011), thus representing a

neuroinflammatory paradigm quite different from the direct LPS intracerebral infusion. Female littermates of the two genotypes were immunized following a standard protocol, and animals were scored for the development/remission of their clinical symptoms over the course of a month (Borroto et al, 2016). Animals were classified with a standard 0 to 5 rank based on their paralysis degree, with 0 corresponding to the absence of symptoms and 5 to a moribund condition (Borroto et al, 2016). In wt mice (n = 19), tail limping—the first symptom of the disease—became apparent around 8 days after immunization with a subsequent rapid progression so that, by 16 days, most of the wt animals presented hindlimb paralysis followed by a slow recovery (Fig 3A). Notably, 47% of the immunized wt mice developed extreme and protracted symptoms (Fig 3A and B). The response of Sfrp1^{−/−} mice (n = 19) to immunization was instead slower and milder: only 16% of them developed extreme symptoms, and their recovery was significantly faster (Fig 3A and B). Immunostaining of spinal cord sections before immunization showed no difference between wt and Sfrp1^{−/−} in astrocytes, microglia or myelin distribution (not shown). In contrast, in animals (n = 4) sacrificed 16 days after immunization, there was a significant reduction in pathological signs in Sfrp1^{−/−} vs wt mice, including infiltration of CD4^{+}/Iba^{-} lymphocytes (no CD4^{+}/Iba^{+} monocytes were instead detected), presence of Iba1^{+} macrophages/activated microglial cells and loss of MBP^{+} myelin (Fig 3C and D). There was no significant difference in the amount of GFAP labelling between wt and Sfrp1^{−/−}; however, in all null mice analysed there was basically no disruption of the astrocytic pial surface otherwise observed in all wt mice (Fig 3C).

All in all, these data indicate that SFRP1 is commonly required for a robust neuroinflammatory response, likely contributing to astrocyte-to-microglia crosstalk.

Astrocyte-derived Sfrp1 is required for a robust response of microglial cells to damage

The latter possibility found support in the observation that astrocytes but not microglial cells are the main SFRP1 source in the brain, although the protein has a widespread distribution including around microglial cells (Fig 1), as well as in the remarkably poor microglial activation (Figs 2 and 3) and myeloid cell recruitment (Fig 3C) observed in the absence of Sfrp1. To further explore this possibility, we used flow cytometric analysis to determine the proportion of the different CD11b^{+} myeloid populations (Greter et al, 2015) in the cortex of CX₃CR1[+/GFP] and CX₃CR1[+/GFP]; Sfrp1^{−/−} mice 3 days after intracerebroventricular LPS or saline administration (Figs 4A and EV2A). In the absence of Sfrp1, there was a significant decrease in LPS-induced infiltration of CD11b^{+}/CD45^{+}/GFP^{−} monocytes and in the proportion of microglial cells that passed from a CD11b^{+}/CD45^{lo}/GFP^{+} surveying to a CD11b^{+}/CD45^{hi}/ GFP^{+} activated state (Figs 4A and B, and EV2A). Furthermore, FACS analysis of isolated GFP-positive microglial cells (Fig EV2B–D) revealed that, upon infusion of pHrodo E.coli BioParticles (Kapellos et al, 2016) into the third ventricle, CD11b^{+}/CD45^{hi}/ GFP^{+} activated microglial cells derived from CX₃CR1[+/GFP]; Sfrp1^{−/−} mouse brains showed less cumulative phagocytized fluorescent signal than those isolated from CX₃CR1[+/GFP] brains at both 40 and 65 h post-infusion (Figs 4C and EV2B–D), whereas CD11b^{+}/CD45^{lo}/GFP^{+} surveying microglial cells showed a very limited phagocytic activity in both genotypes
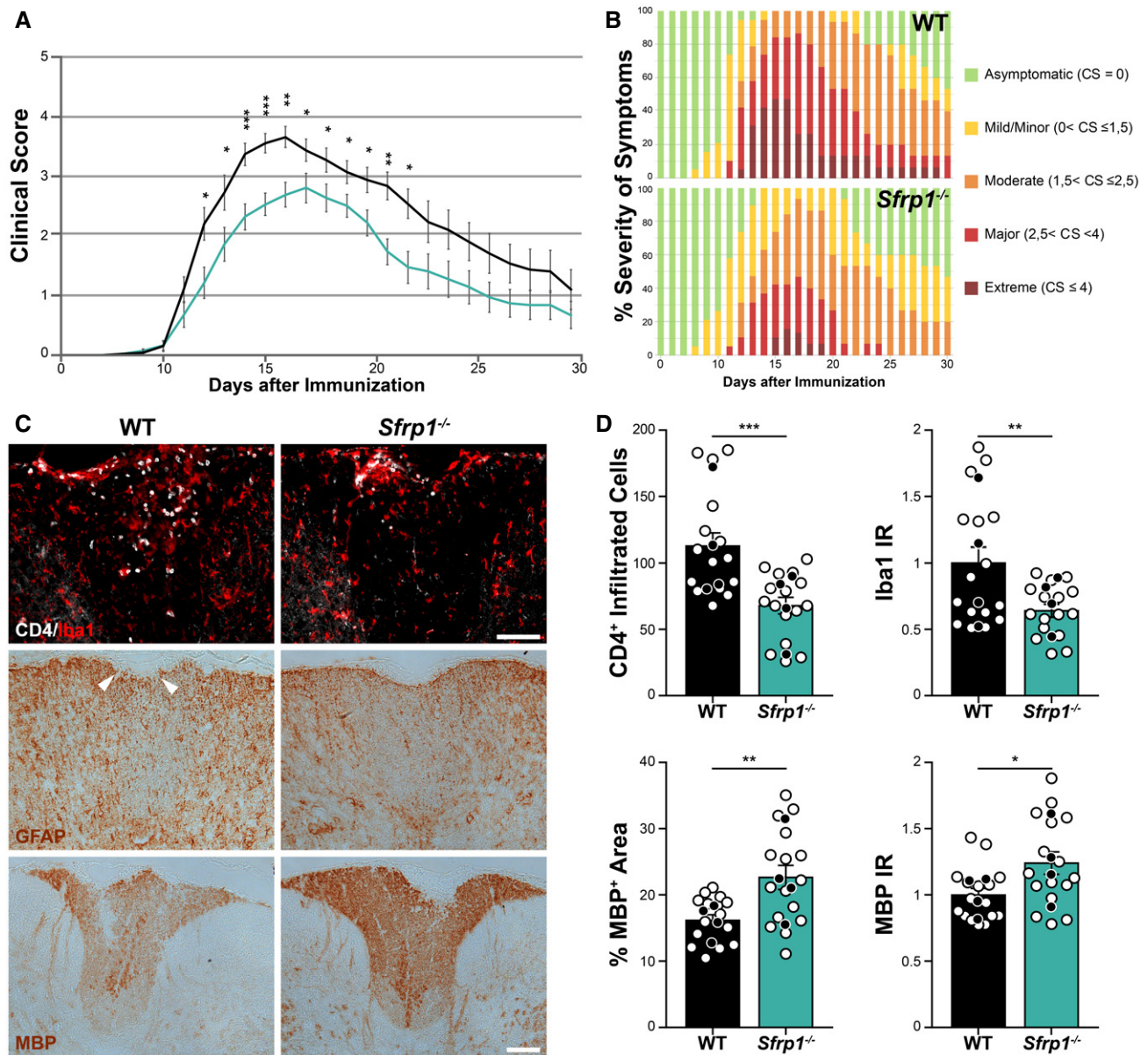
Figure 3. *Sfrp1*$^{-/-}$ mice develop a milder form of EAE.

A, B   Time course analysis and severity of the symptoms in wt and *Sfrp1*$^{-/-}$ mice after EAE induction. In A, means are depicted with black (wt, $n = 19$) and cyan (*Sfrp1*$^{-/-}$, $n = 19$) lines. In B, data are expressed as % of the total number of analysed animals ($n = 19$ per genotype). In (A), error bars represent standard error.

C   Wt and *Sfrp1*$^{-/-}$ mice immunized with MOG and sacrificed 16 days post-immunization. Cryostat sections of the thoracic spinal cords were stained with antibodies against CD4, Iba1, GFAP and MBP. Images show the region dorsal fasciculus. White arrowheads point to the disruption of the pia surface in wt. Scale bar: 100μm.

D   Quantification of CD4$^+$ infiltrated lymphocytes, Iba1-normalized immunoreactivity, MBP-normalized immunoreactivity and MBP immune-reactive area in the dorsal fasciculus of spinal cord sections from wt and *Sfrp1*$^{-/-}$ mice 16 days after immunization ($n = 16$ acquisitions, white dots; from $N = 4$ animals, black dots, per genotype). Error bars represent standard error. Statistic refers to number of acquisitions.

Data information: $*P < 0.05$, $**P < 0.01$ and $***P < 0.001$ by the Kolmogorov–Smirnov test followed by the Mann–Whitney U nonparametric test comparing mice of the same day after immunization (A) or two-sided Student's t-test (D).

(Fig EV2B). Notably, at 40 h the percentage of phagocyting microglial cells in *CX$_3$CR1*$^{+/GFP}$; *Sfrp1*$^{-/-}$ mice was significantly higher than in controls (Fig 4C), but this proportion underwent a drastic reduction at 65 h (Fig 4C). These data suggest that in the absence of SFRP1, microglial cells present a less efficient phagocyting activity

that, at earlier time points, might be compensated by increasing cell recruitment. A differential rate of phagocytosis vs degradation or the acidity of the lysosomal compartment (Sole-Domenech *et al*, 2016) may also explain the time course of phagocytosis and the lower phagocytic signal observed in mutant microglia.
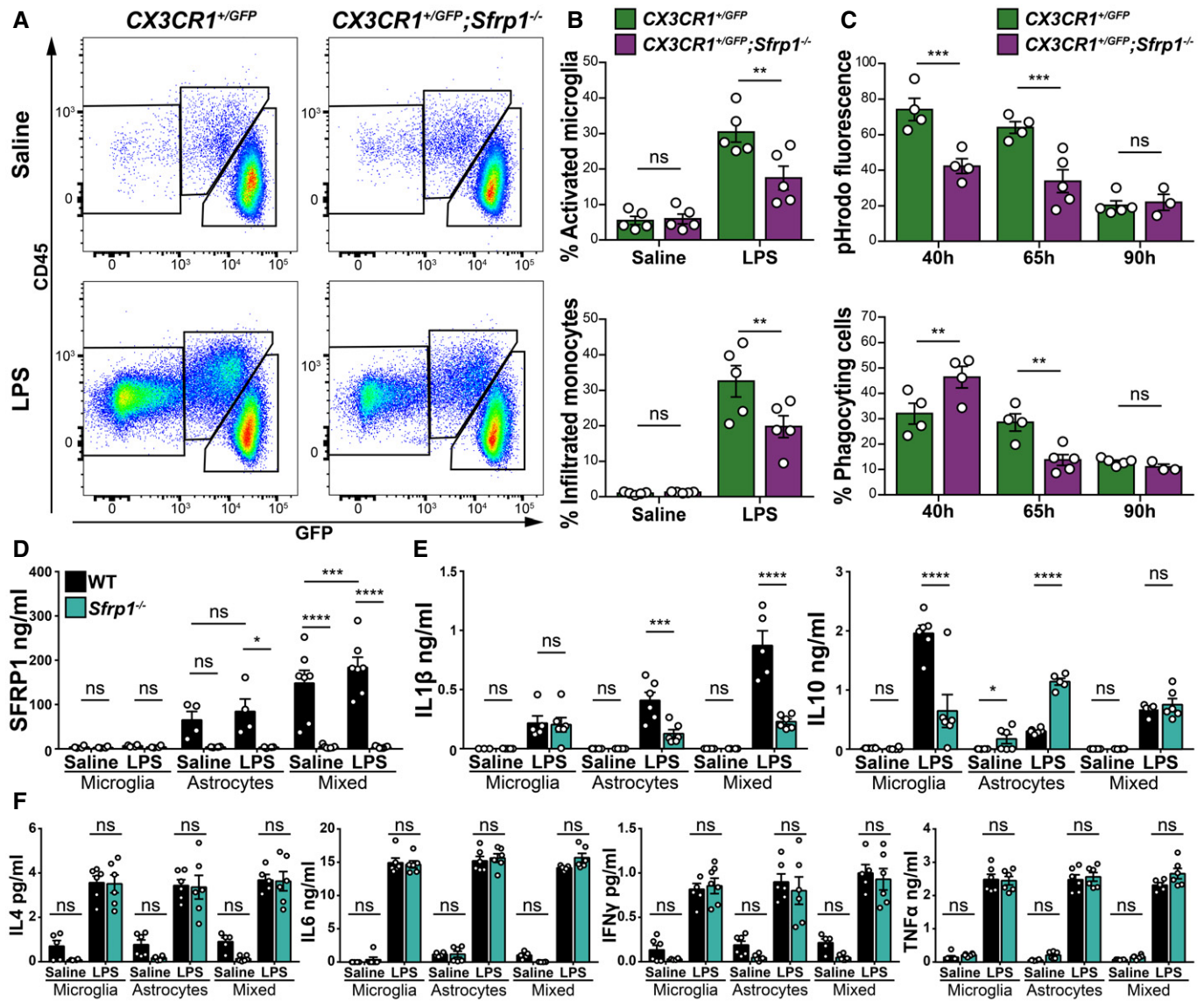
Figure 4. SFRP1 amplifies LPS-induced microglial activation and modifies their cytokine secretion.

A   Representative cytometric plots of CD11b+ populations present in the cortex of $CX_3CR1^{GFP/+}$ or $CX_3CR1^{GFP/+};Sfrp1^{-/-}$ mice 3 days after saline or LPS intraventricular infusion. Gating was set for isolating the following myeloid cell populations: CD11b$^+$; CD45^{lo}; GFP$^+$ surveying microglia, CD11b$^+$; CD45$^+$; GFP$^+$ activated microglia and CD11b$^+$;CD45$^+$;GFP$^-$ infiltrated monocytes.

B   Quantification of the percentage of activated microglia and infiltrated monocyte present in $Sfrp1^{-/-}$ and controls brains 3 days after infusion of saline or LPS ($n = 5$ animals per genotype and condition). Error bars represent standard error. Statistical significance: **$P < 0.01$ by two-way ANOVA followed by Bonferroni's multiple comparisons test.

C   Quantification of the total fluorescence from phagocytized pHrodo-labelled *E. coli* BioParticles and percentage of phagocyting cells in the CD11b$^+$;GFP$^+$ microglial population ($n = 3$–5 animals per genotype and condition). Error bars represent standard error. Statistical significance: **$P < 0.01$ and ***$P < 0.001$ by two-way ANOVA followed by Bonferroni's multiple comparisons test.

D   ELISA determination of SFRP1 levels present in the media of microglia ($n = 4$ cultures per genotype), astrocytes ($n = 4$ cultures per genotype) or mixed astrocytes and microglial (2:1, $n = 7$ cultures per genotype) cultures derived from wt or $Sfrp1^{-/-}$ pups exposed for 24 h to saline or LPS (1 μg/ml). Error bars represent standard error. Statistical significance: *$P < 0.05$, ***$P < 0.001$ and ****$P < 0.0001$ by one-way ANOVA followed by the Bonferroni test.

E, F Secretory profile of cytokines present in the medium of microglia, astrocytes or mixed astrocytes and microglial (2:1) culture as above ($n = 5$–6 cultures type—microglia, astrocytes or mixed cultures—and genotype). The content of IFN-γ, TNF-α, IL-1β, IL-4, IL-6 and IL-10 was determined by multiplex ELISA. Values are represented in absolute concentration. Error bars represent standard error. Statistical significance: ns, $P > 0.05$, *$P < 0.05$, ***$P < 0.001$ and ****$P < 0.0001$ by two-way ANOVA followed by Bonferroni's multiple comparisons test.

This effect could be direct or mediated by a more complex mechanism associated with SFRP1-producing astrocytes. To test these possibilities, we exposed wt microglial cell suspensions to pHrodo

E. coli BioParticles in the presence or absence of wt or $Sfrp1^{-/-}$ astrocytes. After 1-h incubation, the presence of phagocytized fluorescent signal of CD11b$^+$ microglial cells was evaluated by FACS

analysis. In the presence of $Sfrp1^{-/-}$ astrocytes, both the phagocytized fluorescent signal and the proportion of phagocyting microglial cells were lower than those observed in the presence of wt astrocytes (Fig EV2E). Although in both cases the difference was not significant, this observation points to a cell non-autonomous effect.

Collectively, these data support the contention that astrocyte-derived SFRP1 modulates microglial activation in response to an inflammatory challenge and favours their efficient function. To assess that there is indeed an astrocyte-to-microglial flux of information, we next established microglia, astrocyte or astrocyte–microglia mixed cultures (2:1, close to the reported ratio existent in the mouse cortex; Keller et al, 2018) from wt and $Sfrp1^{-/-}$ neonatal mouse cortices, using the same density in each case. ELISA determination confirmed the presence of SFRP1 only in culture media from wt astrocytes or mixed cultures, which was increased after LPS treatment (Fig 4D), further supporting the astrocytic origin of SFRP1 and the notion that SFRP1 levels increase upon an inflammatory stimulus. Notably, in the mixed culture, although the total amount of astrocytes was one third less than that present in the pure astrocytic cultures, SFRP1 levels were significantly increased in both the presence and absence of LPS (Fig 4D), suggesting that microglia somehow influences SFRP1 secretion. We next used a multiplex ELISA to determine cytokines' release (IFN-γ, TNF-α, IL-1β, IL-4, IL-6 and IL-10) in the media of the three culture types (Fig 4E and F), as a measure of their LPS-induced activation (Heneka et al, 2014). At 24 h, LPS but not saline treatment enhanced the accumulation of all cytokines tested in the culture media of both purified microglia and astrocyte cultures, with no significant differences between genotypes in the case of IFN-γ, IL-4, IL-6 and TNF-α (Fig 4F). $Sfrp1^{-/-}$ astrocytes but not microglial cells produced instead significantly lower levels of IL-1β upon LPS treatment, and this difference was more pronounced in the mixed cultures (Fig 4E). Notably, in the presence of LPS, IL-10 production was significantly increased in the media of $Sfrp1^{-/-}$ astrocytic cultures but decreased in the corresponding microglia media as compared to wt (Fig 4E). These opposite changes likely explain why there was no difference in IL-10 production between wt and mutant mixed cultures.

Taken together, these results indicate that SFRP1 may be both a target and an effector of the astrocyte–microglia crosstalk during inflammation. In particular, astrocyte-derived SFRP1 influences the response of both astrocytes and microglial cells to an inflammatory stimulus, modifying their ability to secrete at least two specific cytokines: IL-1β and IL-10.

Sfrp1 allows for the full expression of downstream targets of HIF transcription factors

We next reasoned that if SFRP1 influences microglial activation, its absence should modify their transcriptomic profiling towards a less activated or surveying state. To test this possibility, we used fluorescence-associated cell sorting to purify GFP$^+$ microglial cells from the brain of $CX3CR1^{+/GFP}$ and $CX3CR1^{+/GFP}$; $Sfrp1^{-/-}$ mice ($n = 4$). Cells were purified three days after the injection of LPS or saline and used to obtain the corresponding transcriptomic profiles. Confirming previous results, $Sfrp1$ mRNA was not detected at any significant levels in the microglial transcriptome independently of the genotype or treatment (Fig EV3A and data deposited in ERP119668/PRJEB3647). We next compared the gene expression

signature of $CX3CR1^{+/GFP}$- and $CX3CR1^{+/GFP}$; $Sfrp1^{-/-}$-derived microglial cells in response to LPS (Fig 5). Principal component analysis (Fig 5A, Dataset EV1A–D) and volcano plot comparisons (Fig EV3B) demonstrated LPS as the main source of variation (72% variance), whereas only 6% of the total variations could be attributed to the genotype after secondary component analysis, well in line with the observation that SFRP1 is poorly expressed in the adult brain under homeostatic conditions (Fig 1; Esteve et al, 2019b). The relatively central position of LPS-treated $Sfrp1^{-/-}$ microglia supported their milder inflammatory response (Figs 2 and 3), which was further confirmed when overall gene expression variations of LPS-treated control and $Sfrp1^{-/-}$ microglia were plotted and compared (Fig 5B and C). Linear regression analysis of this comparison demonstrated a 30% reduction in the global transcriptomic response induced by LPS in the absence of $Sfrp1$ (slope of red dotted line, Fig 5D). LPS treatment in control microglia induced the upregulation of 1,128 genes, 487 of which were shared with $Sfrp1^{-/-}$ microglia (Dataset EV1A–B). LPS treatment also induced the upregulation of 121 and the downregulation of 167 microglial genes in the absence of SFRP1 (Fig 5E; Dataset EV1A–D). Genes associated with metabolic pathways (i.e. *AldoA*, *LdhA* or *Pygl)*, the cell cycle (i.e. *Gas6*) or immune regulators (i.e. *Mif*, *Mefv*) were highly upregulated in controls but not in $Sfrp1^{-/-}$ microglia (Dataset EV1A–D), whereas genes downstream of the Toll-like 4 receptor (TLR4), such as *Tlr2*, were upregulated at similar levels in both genotypes (Dataset EV1A–D). TLR4 is fundamental for LPS recognition and the activation of the immediate inflammatory response (Ransohoff & Perry, 2009), strongly suggesting that, in the absence of $Sfrp1$, microglial cells retain their prompt response to damage.

Consistent with this observation, hierarchical clustering of the samples demonstrated treatment-dependent similarities, but with $Sfrp1^{-/-}$ microglia showing an attenuated response to LPS treatment as compared to wt (Fig 5F). Hierarchical clustering of the differentially expressed genes presented a pattern of covariance that was further analysed by Z-score covariance unsupervised clustering (Fig 5F). This analysis generated 4 different clusters of upregulated genes, which were analysed for enrichment of regulatory elements and gene ontology annotations (Fig EV4). Genes regulated by E2F transcription factors and implicated in cell cycle regulation composed the less abundant 3 and 4 clusters. Genes belonging to cluster 3, involved in the regulation of chromosomal segregation and spindle organization, were slightly more upregulated in control microglia. On the contrary, genes belonging to cluster 4 and involved in chromatin assembly and DNA packing were upregulated in $Sfrp1^{-/-}$ microglia, suggesting possible differences in the length of the cell cycle (Fig EV4).

Clusters 1 and 2 were the largest clusters and included genes that mediate the inflammatory response and regulators of the defence response (Fig EV4A and B). Both clusters were strongly upregulated in control microglia in response to LPS (Fig EV4A): genes in cluster 1 showed significant enrichment in NF-kB TF binding sites at the promoter regions, whereas those putatively controlled by HIF transcription factors were enriched in cluster 2 (Fig EV4C; Table EV1E–F). In microglia derived from $Sfrp1^{-/-}$ mice, the expression of a few genes belonging to cluster 1 was decreased (Fig EV4A; Dataset EV1E–F), whereas that of genes belonging to cluster 2 was basically abrogated (Fig EV4A; Dataset EV1E–F). Ingenuity Pathway Analysis network representation of the NF-κB and HIF downstream targets
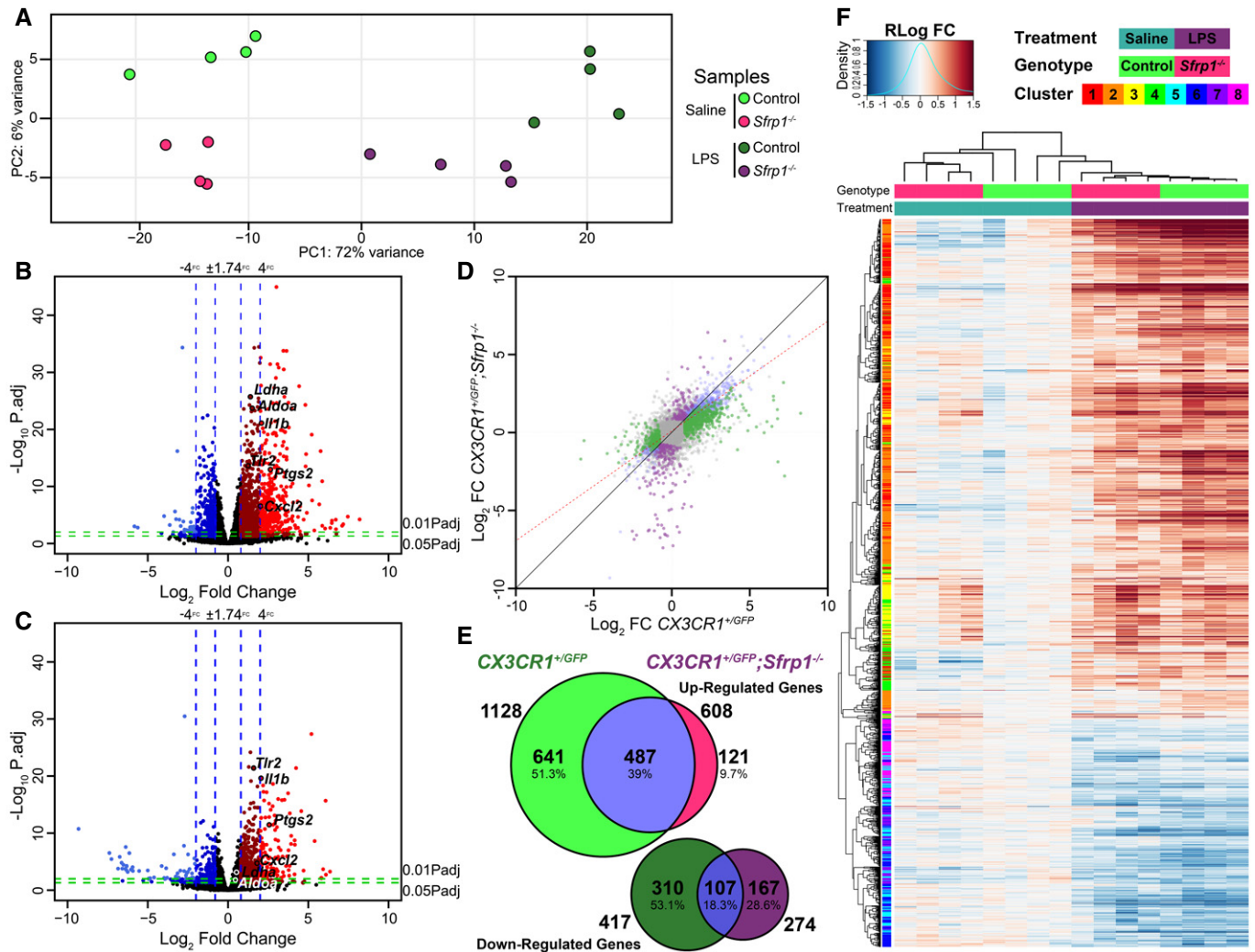
Figure 5. SFRP1 enhances microglial cells' transcriptional response to LPS treatment.

A   Principal component analysis with the 1,000 most variable genes from microglial cells isolated from $CX_3CR1^{GFP/+}$ and $CX_3CR1^{GFP/+};Sfrp1^{-/-}$ mouse brains three days after saline or LPS intracerebroventricular infusion. The analysis depicts sample clusterization by genotype and treatment.

B, C   Volcano plots of differential gene expression from $CX_3CR1^{GFP/+}$ (B) or $CX_3CR1^{GFP/+};Sfrp1^{-/-}$ (C) microglial cell in response to LPS. Data are represented as log2 fold change vs -Log10 adjusted P-value by the Wald test corrected for multiple comparisons by the Benjamini and Hochberg method. Blue vertical lines represent an increase of 75 and 400% in the expression levels, respectively. Green horizontal lines represent a 0.05 or 0.01 adjusted P-value of statistical significance, respectively. Genes with an expression change higher than 75% and an adjusted P-value lower than 0.05 are highlighted in dark red (+FC) and dark blue (−FC). Genes with an expression change higher than 400% and an adjusted P-value lower than 0.01 are coloured in light red (+FC) and light blue (−FC).

D   Scatterplot of differentially expressed genes in $CX_3CR1^{GFP/+}$ and $CX_3CR1^{GFP/+};Sfrp1^{-/-}$ microglia; the red line represents linear regression (slope 0.704014 P-value: < 2.2e-16 by the F-test followed by Bonferroni's correction) of the differential expression, indicating response attenuation. Coloured dots represent response, which are exclusive for each genotype as represented in (E).

E   Venn diagram showing the extent of differential gene expression in response to LPS in $CX_3CR1^{GFP/+}$ or $CX_3CR1^{GFP/+};Sfrp1^{-/-}$ microglial cells. Fold change (75%) and adjusted P-value < 0.05 cut-off by the Wald test corrected for multiple comparisons by the Benjamini and Hochberg method.

F   Heatmap showing fold changes of regularized log-transformed gene-level RNA-seq counts with hierarchical clustering of samples and differentially expressed genes in response to LPS in $CX_3CR1^{GFP/+}$ or $CX_3CR1^{GFP/+};Sfrp1^{-/-}$ microglial cells.

showed that the absence of SFRP1 has a greater effect on downstream targets of HIF (Fig 6A). Genes downstream NF-κB, such as *Tlr2* and *ApoE,* showed LPS-dependent upregulation with levels almost similar in the two genotypes, whereas the expression of the homeostatic *Cx3cr1* and *Trem2* genes was unchanged (Fig 6B; Dataset EV1E). Of note, a number of genes shared between the NF-κB and HIF pathways, such as *Cxcl2, Cxcl3* and *Ptgs2,* were strongly

upregulated in LPS-treated control microglia but not in those derived from $Sfrp1^{-/-}$ brains (Fig 6A). This difference, albeit at a slightly lower level, was also observed for IL-1β and IL-10 (Fig 6A) supporting the differences observed in cell culture media (Fig 4E). Similarly, other LPS-induced HIF targets failed to be upregulated in the absence of *Sfrp1* and maintained levels of expression comparable to those of saline-treated control microglia (Fig 6A and B;
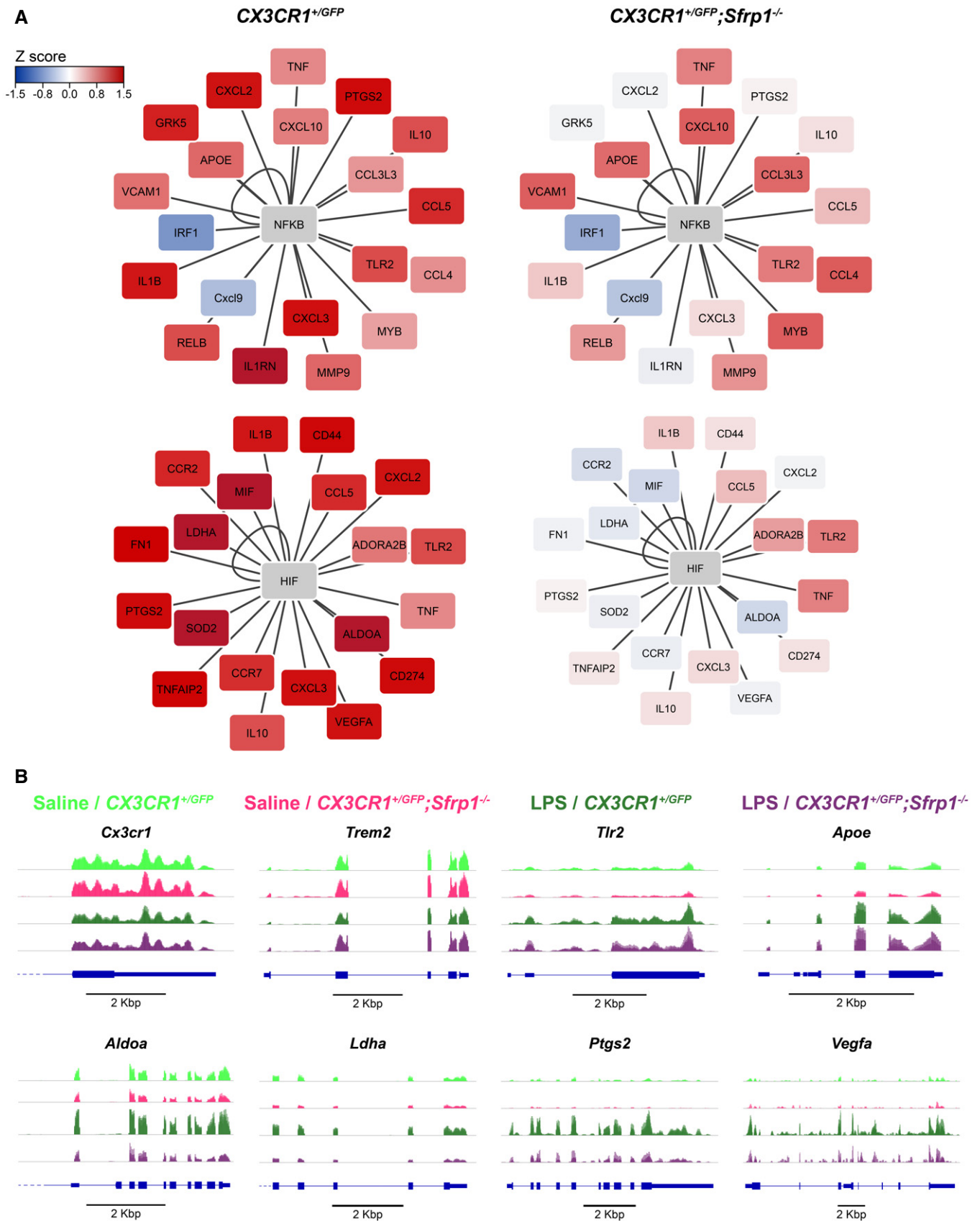
A

B

Figure 6.

Dataset EV1F). These included *Vegfa*, *Sod2*, *Mif*, *Aldoa* and *Ldha*. Notably, *Hif1α* expression was similar to that observed in LPS-treated controls (Dataset EV1F), possibly in line with the notion that Hif1 levels and activity are largely modulated by post-translational modifications and proteolysis (Choudhry & Harris, 2018).

All in all, these results support the idea that in the absence of *Sfrp1*, microglial cells can sense and respond to an inflammatory insult undertaking an initial response. SFRP1 is, however, required to enhance this response allowing for the full activation of microglia-mediated inflammation in the brain.

Discussion

Microglial cells transit from a surveying to an activated state in response to adverse signals derived from the surrounding environment (Kierdorf & Prinz, 2013). However, both insufficient or prolonged microglial activation is harmful to the brain so that an elaborated neuron–microglia–astrocyte crosstalk is in charge of shaping the brain immune response to damage (Colonna & Butovsky, 2017). The molecular components that mediate the flux of information from neurons to microglia (i.e. the CD200/CD200R signalling system) (Kierdorf & Prinz, 2013) or from microglia to astrocytes (i.e. cytokines and NO) (Jha *et al*, 2019) have been in part identified. In contrast, there is perhaps less information on how astrocytes communicate with microglial cells (Jha *et al*, 2019). Our study unveils that SFRP1 is part of the molecular signals that astrocytes provide to microglial cells to enhance their inflammatory response. In response to damage, reactive astrocytes produce and secrete SFRP1, which, in turn, increases the number of activated microglial cells and fosters the expression of HIF and, to a much lower extent, NF-kB downstream targets in microglial cells. SFRP1 persistency is, however, pernicious as it sustains a chronic inflammatory state. Indeed, its inactivation significantly reduces the prolonged neuroinflammation associated with EAE. These observations indicate that SFRP1 is a potential valuable target to counteract the harmful effect of prolonged inflammatory conditions, such as those present in MS or AD.

SFRP1 function has been studied in many developmental contexts largely linked to the control of cell specification, proliferation and differentiation (Bovolenta *et al*, 2008), but its homeostatic role in adult tissues is less clear. Its poor or absent expression (or that of other SFRP family members) due to promoter hypermethylation is considered a sign of bad prognosis in different types of tumour (Dahl *et al*, 2007; Esteve & Bovolenta, 2010; Baharudin *et al*, 2020), although $Sfrp1^{-/-}$ mice are viable, fertile and do not form spontaneous tumour (Trevant *et al*, 2008), indicating that SFRP1 absence per se is not tumorigenic. On the other hand, our finding unveils that elevation of SFRP1 levels has also pathological consequences but related to neuroinflammation (this study) and

neurodegeneration (Esteve *et al*, 2019b). As an advantage, SFRP1 neutralization in AD-like mice counteracts disease pathology without any apparent side effect (Esteve *et al*, 2019b). In the specific case of neuroinflammation, neutralization of SFRP1 function should have less effect on the initial acute inflammatory phase, which is a necessary step towards pathogen elimination, tissue repair and homeostasis restoration (Colonna & Butovsky, 2017). Abrogation of SFRP1 function does not prevent this acute response given that, in its absence, both LPS infusion and MOG immunization induce an initial inflammatory reaction, albeit at somewhat lower levels. Furthermore, activated microglial cells and infiltrated monocytes can still be isolated from the brain of $Sfrp1^{-/-}$ mice, although at significantly decreased numbers. These microglial cells retain phagocytic competence, and no significant difference was observed for most of the LPS-induced cytokines released from purified microglial cells obtained from $Sfrp1^{-/-}$ and wt brains. Nevertheless, the significant less phagocytic efficiency observed *in vivo* and the reduced ability of isolated mutant microglia to secrete IL-10 in response to LPS may be linked to the small (6%) transcriptomic variations observed between control and mutant microglia (Fig 5). This small variation may reflect that astrocyte-derived SFRP1 could influence the development of microglial cells and/or change their behaviour in homeostatic conditions. Although we cannot fully exclude these possibilities, we did not find any significant variations in the number and shape of microglial cells in $Sfrp1^{-/-}$ early postnatal brains and SFRP1 is very poorly expressed in the adult mammalian brain under homeostatic conditions (Esteve *et al*, 2019b, and this study). Our transcriptomic analysis further shows that $Sfrp1^{-/-}$ microglia cells retain their capacity of sensing LPS, providing strong support to the implication of SFRP1 in the amplification of the inflammatory response. Indeed, *Tlr2* expression, a read-out of LPS-mediated TLR4 activation (Rivest, 2009), is increased (and to a comparable extent) in microglial cells from both genotypes. A similar consideration applies to a large fraction of the genes related to the NFκB-dependent pathway, which is largely related to the acute inflammatory response (Kaltschmidt & Kaltschmidt, 2009).

Brain response not only to LPS but also to other harmful signals depends on the fast reaction of functional microglial cells (Holm *et al*, 2012), whereas astrocytes and neurons have a minor role in this response despite their reported expression of the TLR4 receptor (Bowman *et al*, 2003; Rolls *et al*, 2007). Reactive microglial cells thereafter induce astrocyte activation that, in turn, feeds back on microglial function (Jha *et al*, 2019). Fitting our data into this loop, we propose that upregulation and release of SFRP1 from astrocytes occur as part of their microglia-mediated early activation, as supported by the enhanced secreted levels observed when astrocytes and microglial cells were cultured together. Secreted SFRP1 then acts on microglial cells amplifying a HIF-dependent inflammatory response and thus a significant increase in specific cytokine secretion, further impinging upon inflammation. Supporting SFRP1

implication in this astrocyte–microglia loop, astrocytic $Sfrp1^{-/-}$ mice show decreased GFAP expression and thus are also less reactive, likely producing lower levels of other microglia-activating molecules. This implies that, as long as SFRP1 upregulation persists, neuroinflammation persists, contributing to its chronicization. This idea is well in agreement with our observation that genetic inactivation of $Sfrp1$ significantly limits the severity and progression of EAE, a condition that, as MS, is characterized by persistent microglial activation. Both EAE and MS are driven by the infiltration of peripheral macrophages and lymphocytes (Ajami et al, 2011). We cannot exclude that the lack of peripherally expressed $Sfrp1$ may limit this infiltration and thus the disease, especially because SFRP1 has been shown to influence lymphocytes' differentiation (Lee et al, 2012). Notwithstanding, there is strong evidence that endogenous microglial activation is critical for EAE onset and maintenance (Becher et al, 2001; Heppner et al, 2005) and the $SFRP1$ gene is hypomethylated in brain samples from MS patients (Chomyk et al, 2017), likely promoting an abnormal protein increase. Thus, reduced microglial activation is a plausible cause of the milder EAE symptoms observed in $Sfrp1^{-/-}$ mice.

SFRP1 upregulation in other neurodegenerative diseases characterized by the presence of chronic inflammation further supports a role of SFRP1 microglial activation. An example is Glaucoma (Wang et al, 2008) or AD (Esteve et al, 2019b; Bai et al, 2020; preprint: Johnson et al, 2021), in which antibody-mediated neutralization of SFRP1 strongly decreases different AD pathological features, including neuroinflammation (Esteve et al, 2019b). Notably, SFRP1-mediated inhibition of ADAM10 contributes to the generation of toxic amyloid peptides in AD patients, whereas SFRP1 deficiency decreases amyloid burden (Esteve et al, 2019b). Low neuroinflammation upon SFRP1 neutralization could therefore be secondary to this reduction (Esteve et al, 2019b). The present study shows that this is not necessarily the case as SFRP1 acts directly on microglial cells, suggesting that SFRP1 simultaneously impinges upon multiple pathological events in AD. A possible SFRP1-mediated activation of microglial cells in AD finds further support in our transcriptomic analysis that links SFRP1 with HIF signalling. Indeed, many LPS-induced genes regulated or coregulated by HIF were not activated in the absence of $Sfrp1$, although $Hif1\alpha$ expression was not modified, possibly because its levels are largely post-translationally regulated (Choudhry & Harris, 2018). Consistent with our observations, a number of recent studies have shown that microglial cells isolated from AD-like mouse models undergo important metabolic changes with the activation of the HIF pathway (Ulland et al, 2017; Wendeln et al, 2018; Baik et al, 2019). Furthermore, $Hif1\alpha$ is involved in astrocytic proinflammatory activity (Wheeler et al, 2019) and its activity seems to be dysregulated in association with other genes genetically linked to AD risk, suggesting that HIF-1α may be detrimental in AD pathology (Wendeln et al, 2018).

The precise molecular interactions underlying SFRP1-mediated HIF pathway activation are at the moment an open question. Microglial cells express members of the ADAM family of metalloproteases (Kleinberger et al, 2014), including ADAM10, which has been shown to be upregulated in both neurons and microglial cells during microglia-mediated synaptic pruning (Gunner et al, 2019). Furthermore, SFRP1 effectively inhibits ADAM enzymatic activity in cultured microglial cells (our own observations). Given that TREM2 is a proven substrate of ADAM10/17 (Kleinberger et al, 2014), it

seems plausible to postulate that SFRP1 may modulate the shedding of TREM2 on the surface of microglial cells. This shedding occurs, for example, in response to LPS-induced activation of TLR4 (Turnbull et al, 2006; Piccio et al, 2007), thereby attenuating microglial activation (Turnbull et al, 2006). Notably, microglial cells deficient in TREM2 undergo only a partial and abortive activation and remain locked in an almost homeostatic state (Keren-Shaul et al, 2017; Mazaheri et al, 2017). It is thus tempting to speculate that in SFRP1 absence, enhanced shedding of TREM2 may reduce microglial activation as we have observed in $Sfrp1^{-/-}$ mice, whereas high SFRP1 levels, by interfering with ADAM function, may enhance TREM2 signalling. In addition (or alternatively), SFRP1 may interfere with ADAM10-mediated shedding of the neuronal ligands CX3CL1 and CD200 preventing the generation of their soluble forms (Hundhausen et al, 2007; Wong et al, 2016) and thus the activation of their respective microglial receptors, CX3CR1 and CD200R (Jung et al, 2000; Wright et al, 2000). Unfortunately, lack of appropriate biochemical tools has prevented us from verifying these possibilities in our mouse models, leaving this question open for future studies.

An alternative and non-mutually exclusive possibility involves SFRP1 function as a Wnt signalling modulator. The role of this pathway in microglial activation is, however, somewhat controversial, perhaps in line with the notion that Wnt pathway activity is highly context-dependent. For example, studies in $vitro$ have shown that Wnt3a and Wnt5a can counteract LPS-induced microglial activation (Halleskog & Schulte, 2013). In contrast, in preterm-born infants and in different postnatal animal models of injured-induced neuroinflammation, downregulation of the expression of Wnt signalling components seems a prerequisite for proinflammatory activation of microglia (Van Steenwinckel et al, 2019). SFRP1 upregulation could lead to the same net effect, inducing at least the downregulation of the expression of $Axin2$ or $Lef1$, genes that targets and read-out of Wnt/βcatenin pathway activation. Notably, however, we found no evidence of changes in the expression of these genes in our RNA-seq analysis.

In conclusion, we have shown that astrocyte-derived SFRP1 plays an important role in shaping microglial response to CNS damage, sustaining chronic neuroinflammation. This effect might not be limited to the brain, as SFRP1 upregulation has been reported in different pathological conditions associated with inflammation or fibrosis such as periodontitis, rheumatoid arthritis, uropathies or pulmonary emphysema (Esteve & Bovolenta, 2010; Claudel et al, 2019). Therefore, once analysed the possible side effect, SFRP1 neutralization (Esteve et al, 2019b) may represent a promising therapeutic avenue to treat a wide variety of chronic pathological conditions.

Materials and Methods

Animals

Newborn and adult mice of both sexes were used, unless otherwise indicated. Mice were maintained in pathogen-free conditions at the CBMSO animal facilities, following current national and European guidelines (Directive 2010/63/EU). Experimental procedures were approved by the CBMSO and Comunidad Autónoma de Madrid ethical committees. $Sfrp1^{-/-}$ mice were generated by inter-cross of the

$Sfrp1^{-/-}$; $Sfrp2^{+/-}$ mice in a mixed 129/C57BL/6 background as described (Esteve *et al*, 2011a) and then back-crossed at least 4X with C57BL/6J to unify the background. Wild-type (wt) animals were littermates selected from heterozygous crosses. Breeding pairs of $CX_3CR1::GFP$ mice (Jung *et al*, 2000) were kindly provided by Prof. J Avila, CBMSO. Mice were further crossed with the $Sfrp1^{-/-}$ to obtain $CX_3CR1::GFP$; $Sfrp1^{-/-}$.

Stereotactic LPS infusion

LPS or saline was infused into the brain parenchyma of 10- to 12-week-old littermates from wt and $Sfrp1^{-/-}$ or $CX_3CR1^{+/GFP}$ and $CX_3CR1^{+/GFP}$; $Sfrp1^{-/-}$ mice. Animals were anaesthetized with 4% Isoflurane (Forane, AbbVie Farmacéutica) vaporized into a sealed anaesthetic induction chamber (SurgiVet, Smiths Medical) and placed in a stereotaxic apparatus (Stoelting). Anaesthesia was maintained at 2.5% in 250 ml/min oxygen flow. Saline (2.5 μl) or LPS (5 μg; *Escherichia coli* 0111:B4; Sigma-Aldrich) was delivered through a small skull window using a Quintessential Stereotaxic Injector (Stoelting) coupled to a 10 μl syringe with a 34G needle (Hamilton) at the rate of 0.5 μl/min using the following bregma coordinates: 0.0 mm A-P; −1.0 mm lateral, and −1.5 mm D/V. Mice were let survive for three days and then sacrificed and processed for further analysis. Delivery of pHrodo Red *E. coli* BioParticles Conjugate (Molecular Probes) was performed with a similar procedure at −2.5 mm A-P; 0.0 mm lateral, and −2.3 mm D-V from bregma. Lentiviral vectors (2.5 μl), generated as described below, were delivered −0.5 mm A-P; 1.0 mm lateral and −2.3 mm D-V from bregma. Mice were let survive 1–5 months and then analysed.

Lentiviral (LV) particle generation

LV particles carrying IRES-*Gfp* or *Sfrp1*-IRES-*Gfp* were obtained by transient transfection of mycoplasma-free HEK-293T cells (Marin *et al*, 2016; Merten *et al*, 2016). Cells were transfected employing a three-plasmid HIV-derived and VSV-pseudotyped LV system kindly provided by M.K. Collins, University College London, UK; A. Thrasher, Institute of Child Health, UK; and D. Trono, Ecole Polytechnique Fédérale de Lausanne, Switzerland. Culture supernatants were collected two and three days after transfection and ultracentrifuged. Pellets containing the concentrated particles were resuspended in PBS. Functional titre of the viral preparations was determined by transfection of HEK-293T cells (1×10^8 TU/ml, in both cases).

Experimental Autoimmune Encephalomyelitis (EAE)

Chronic EAE was induced as described (Borroto *et al*, 2016). Briefly, 8- to 10-week-old female C57BL/6J and $Sfrp1^{-/-}$ littermates were injected bilaterally in subcutaneous femoral region with 150 mg of MOG35–55 (Espikem) emulsified with Freund's complete adjuvant (Sigma-Aldrich), supplemented with Mycobacterium tuberculosis (1mg/ml; H37Ra strain from Difco), followed by two intraperitoneal injections of pertussis toxin (200 ng; Sigma-Aldrich) separated by 48h. An observer blind to the animals' genotype weighed and inspected the animals daily to detect the appearance of clinical signs according to the following classification: (0) no overt signs of disease; (1) weakness at the tail distal portion; (1.5) complete tail flaccidity;

(2) moderate hindlimb weakness; (2.5) severe hindlimb weakness; (3) ataxia; (3.5) partial hindlimb paralysis; (4) complete hindlimb paralysis; (4.5) complete hindlimb paralysis with muscle stiffness; and (5) moribund state and hence sacrificed according to the ethical procedures. A representative pool of mice was anaesthetized and perfused intracardially sixteen days after immunization, when symptoms picked, for histological analysis. Other animals were let recover. Spinal cords were dissected and processed.

Primary cultures

Glial primary cultures were established from cerebral cortices of C57BL/6J or $Sfrp1^{-/-}$ 1- to 3-day-old pups dissected in Ca^{2+}/Mg^{2+}-free Hank's Balanced Salt Solution (HBSS, Invitrogen) and processed following the standard procedures (Bovolenta *et al*, 1993). Cells were plated in Dulbecco's modified Eagle's medium and F12 nutrient mixture (DMEM/F12, Invitrogen) containing 10% FCS (Invitrogen) and gentamycin (Sigma-Aldrich). Cortices from two pups were platted in a 75-cm^2 flask pretreated with Poly-D-Lys (P7280, Sigma-Aldrich) and cultured at 37°C in a humidified 5% CO_2 incubator. After 24h, the medium was refreshed and supplemented with m-CSF1 to improve microglial survival. Cultures were let reach confluency (about 2 weeks) without further changes. Microglial cells were purified by mechanical detachment of mixed glial cultures (3 h at 37°C and 150 rpm), recovered by medium centrifugation (5 min; 1,000 rpm) (Bovolenta *et al*, 1993) and plated replacing only 50% of the medium to promote microglial proliferation. Astrocytes were instead recovered after two consecutive trypsin–EDTA treatments (0.25% trypsin (Invitrogen), 1 mM EDTA in PBS at 37°C for 3 and 15 min) in which cells recovered after first treatment were discarded. After adding DMEM/F12 with 10% FCS, cells were centrifuged for 5 min at 1,000 rpm and resuspended in the same medium. Mixed cultures were established from the isolated astrocyte–microglia population using a ratio of 2:1 to reflect the reported proportion present in the mouse cortex (Keller *et al*, 2018). In each case, cells were seeded on multiwell culture plates (Falcon) at the final density of 10^5 cells/cm^2. Cells were let settle for 48h and thereafter treated with either LPS (1 μg/ml) or saline in DMEM/F12 without serum. After 24 h of treatment, the cell media were then collected and analysed.

Immunohistochemistry

Adult mice were perfused transcardially with 4% PFA in PB 0.1 M (wt/vol). Brains were removed, post-fixed by immersion overnight and then washed for 24 h in PBS, on a rocking platform at 4°C. Spinal cords were extracted after body post-fixation and washing. Tissues were incubated in a 30% sucrose-PB solution (wt/vol) for 24 h, embedded in a 7.5% gelatine and 15% sucrose solution (wt/vol), frozen on dry ice and, if necessary, stored at −80°C until serially sectioned coronally at 15 μm of thickness using a cryostat (Leica). Histological and cytological immunostaining was performed following standard protocols, after antigen retrieval (10 mM citrate buffer, pH6, for 5 min at 110°C in a boiling chamber, Biocare Medical). Primary antibodies (Table EV1) were incubated ON at RT. The following secondary antibodies were incubated for 1h at RT: Alexa 488- or Alexa 594-conjugated donkey anti-rabbit or anti-mouse (1:1,000); goat anti-rat (1:3,000; Molecular Probes, Invitrogen) or

anti-chicken (1:2,000, Abcam); biotin-conjugated goat anti-mouse or anti-rabbit (1:500, Jackson Lab); Alexa 488 and Alexa 594 (1:500; Molecular Probes, Invitrogen); or POD-conjugated (Jackson Lab) streptavidin followed by reaction with 3,3-diaminobenzidine (0.05 %; Sigma) and 0.03 % H_2O_2. For immunofluorescence, sections were counterstained with Hoechst (Sigma-Aldrich). Tissue was analysed with a DMCTR5000 microscope equipped with a DFC350Fx monochrome camera or a DFC500 colour camera (Leica Microsystems) or with a LSM710 confocal imaging system coupled to an AxioImager.M2 vertical microscope (Zeiss) or a LSM800 coupled to an Axio Observer inverted microscope (Zeiss). Fluorescence was quantified with ImageJ software (National Institute of Health) using 12–14 sections per analysed brain.

ELISA

The levels of specific cytokines present in the glial culture media were determined by electrochemiluminescence using 96-well V-PLEX plates for proinflammatory mouse panel 1 (K15048D) or custom mouse cytokine V-PLEX plates for IFN-γ, IL-1β, IL-4, IL-6, IL-10 and TNF-α, following the manufacturer's indications and using a Quick-Plex SQ 120 reader (Meso Scale Discovery). SFRP1 presents in glial culture medium or in the RIPA fraction of brain lysates was determined with a capture ELISA (Esteve *et al*, 2019b). Culture media were diluted five-fold, and brain lysates used at 0.1 μg/μl protein concentration were determined with BCA protein assay (Thermo Scientific). Values were determined at 450-nm wavelength using a FLUOstar OPTIMA microtitre plate reader (BMG LABTECH).

Fluorescence-Activated Cell Sorting (FACS) and flow cytometric analysis

$CX_3CR1^{+/GFP}$ and $CX_3CR1^{+/GFP}$; $Sfrp1^{-/-}$ 10- to 12 week--old male littermates were treated with LPS or saline as described. After 3 days, animals were perfused with ice-cold saline and brains collected on ice-cold, HBSS Ca^{2+}, Mg^{2+}-free (Invitrogen). After meninges' removal, cortices were isolated, finely chopped and digested for 20 min in DMEM with GlutaMAX (Invitrogen) containing papain 20 U/ml (Worthington Biochemical Corporation), DNase (50 U/ml, Sigma-Aldrich) and L-cysteine (1 mM, MERCK). After addition of 20% FCS (Invitrogen), the tissue was mechanically dissociated and filtered through a 35-μm nylon strainer (Falcon). Microglial cells were separated from myelin/debris by isotonic Percoll gradient centrifugation (35% Fisher Scientific) at 1,200 *g* for 45 min at 4°C. The pellet was recovered and sequentially incubated with anti-mouse CD16/CD32 (1:250, BD Pharmingen; for 15 min at 4°C) followed by rat anti-CD11b and PerCP-Cy5.5 rat anti-mouse CD45 (1:200, BD Pharmingen; for 30 min at 4°C), all in 2% BSA, 5mM EDTA in PBS. After washing, cells were sorted using a BD FACSAria Fusion Flow Cytometer and their signal, size and complexity acquired with DiVA8 Software (BD Pharmingen). Analysis was performed using FlowJo v10.0.7 Software (BD Pharmingen).

Determination of phagocytic activity

The content of pHrodo Red *E. coli* BioParticles (Molecular Probes) in CD11b-positive microglial cells was quantified by FACS using 561-nm excitation/585-nm emission maxima following the manufacturer's recommendations. The gating strategy is described in Fig EV2. When analysis was performed in cultured cells, microglial cells and astrocytes were harvested separately as described in the primary cultured methods, mixed (1:2) and then incubated with pHrodo BioParticles (5 μg/ml) for 1 h. Afterwards, cells were washed and labelled with CD11b, counterstained with DAPI and analysed by FACS.

Genomic data processing and access

RNA from sorted microglia was extracted with the TRI reagent (MERCK) according to the manufacturer's instructions, and purified with RNeasy Lipid Mini Kit (Qiagen) following the manufacturer's protocol, and the resulting total RNA was treated with RNase-Free DNase Set (Qiagen). RNA quality was assessed with a Bioanalyzer 2100 system (Agilent), obtaining RIN (RNA integrity number) values between 8.8 and 10. Each sample (microglia sorted from a single mouse brain) was processed to obtain a RiboZero Stranded Gold Library (Illumina) and sequenced in HiSeq 4000 sequencer in paired-end configuration with 150-bp sequence reads (Illumina). Sequence quality was determined with FastQC (Babraham Bioinformatics) revealing more than 32 million mean cluster reads of over 38 quality score and 93% mean Q30. Reads were aligned with HISAT2 v2.1.0 (Kim *et al*, 2019) to Ensemble *Mus musculus* (GRCm38.94). Aligned reads were further processed using Samtools v1.9 (Li *et al*, 2009) and quantified to gene level using HTseq v0.11.2 (Anders *et al*, 2015). Whole-genome alignments were visualized with Integrative Genomics Viewer (IGV v2.5) (Thorvaldsdottir *et al*, 2013). Differential expression analysis (DGE) was performed using the Bioconductor package DESeq2 v1.10.0 (Love *et al*, 2014). DGE data were processed with custom R scripts (R version 3.5.1, 2018) considering genes with adjusted *P*-value < 0.05 and log2 fold change > ± 0.8 as significantly up- or downregulated. Analysis of GO terms was performed with the Bioconductor package clusterProfiler (Yu *et al*, 2012) and that of promoter-based motif enrichment with HOMER (Heinz *et al*, 2010). RNA-seq data sets can be accessed at the European Nucleotide Archive public repository under the following accession numbers (PRJEB36471/ERP119668).

Statistical analysis

Statistical analysis was performed using Prism v7 software (GraphPad). Different statistical tests were used as indicated in each figure footnote and represented by *P < 0.05, **P < 0.01, ***P < 0.001, and ****P < 0.0001.

Data availability

RNA-seq data sets can be accessed at the European Nucleotide Archive public repository under the following accession numbers (PRJEB36471/ERP119668) at: https://www.ebi.ac.uk/ena/browser/view/PRJEB36471.

Expanded View for this article is available online.

Author contributions

JRC, PE and PB conceptualized and designed the research study. JRC, MJMB, GP and MIM conducted the experiments and acquired the data. AB, JRC and BA designed the EAE study. JRC and AB conducted and analysed the study. JRC, GP, MIM, MTH, PE and PB analysed and discussed the data. FB performed cytokine analysis with the support of MPK and SS. JPLA supervised RNA-seq analysis. JRC and PB wrote the manuscript. All authors read and approved the manuscript.

Conflict of interest

The authors declare that they have no conflict of interest.

References

Aghaizu ND, Jin H, Whiting PJ (2020) Dysregulated Wnt signalling in the Alzheimer's brain. *Brain Sc* 10: 902

Ajami B, Bennett JL, Krieger C, McNagny KM, Rossi FM (2011) Infiltrating monocytes trigger EAE progression, but do not contribute to the resident microglia pool. *Nat Neurosci* 14: 1142–1149

Anders S, Pyl PT, Huber W (2015) HTSeq–a Python framework to work with high-throughput sequencing data. *Bioinformatics* 31: 166–169

Augustine C, Gunnersen J, Spirkoska V, Tan SS (2001) Place- and time-dependent expression of mouse sFRP-1 during development of the cerebral neocortex. *Mech Dev* 109: 395–397

Bachiller S, Jiménez-Ferrer I, Paulus A, Yang Y, Swanberg M, Deierborg T, Boza-Serrano A (2018) Microglia in neurological diseases: a road map to brain-disease dependent-inflammatory response. *Front Cell Neurosci* 12: 488

Baharudin R, Tieng FYF, Lee LH, Ab Mutalib NS (2020) Epigenetics of SFRP1: the dual roles in human cancers. *Cancers* 12: 445

Bai B, Wang X, Li Y, Chen P-C, Yu K, Dey KK, Yarbro JM, Han X, Lutz BM, Rao S *et al* (2020) Deep multilayer brain proteomics identifies molecular networks in Alzheimer's disease progression. *Neuron* 105: 975–991.e7

Baik SH, Kang S, Lee W, Choi H, Chung S, Kim JI, Mook-Jung I (2019) A breakdown in metabolic reprogramming causes microglia dysfunction in Alzheimer's disease. *Cell Metab* 30: 493–507.e6

Becher B, Durell BG, Miga AV, Hickey WF, Noelle RJ (2001) The clinical course of experimental autoimmune encephalomyelitis and inflammation is controlled by the expression of CD40 within the central nervous system. *J Exp Med* 193: 967–974

Blalock EM, Geddes JW, Chen KC, Porter NM, Markesbery WR, Landfield PW (2004) Incipient Alzheimer's disease: microarray correlation analyses reveal major transcriptional and tumor suppressor responses. *Proc Natl Acad Sci U S A* 101: 2173–2178

Borroto A, Reyes-Garau D, Jimenez MA, Carrasco E, Moreno B, Martinez-Pasamar S, Cortes JR, Perona A, Abia D, Blanco S *et al* (2016) First-in-class inhibitor of the T cell receptor for the treatment of autoimmune diseases. *Sci Transl Med* 8: 370ra184

Bovolenta P, Esteve P, Ruiz JM, Cisneros E, Lopez-Rios J (2008) Beyond Wnt inhibition: new functions of secreted Frizzled-related proteins in development and disease. *J Cell Sci* 121: 737–746

Bovolenta P, Wandosell F, Nieto-Sampedro M (1993) Neurite outgrowth inhibitors associated with glial cells and glial cell lines. *NeuroReport* 5: 345–348

Bowman CC, Rasley A, Tranguch SL, Marriott I (2003) Cultured astrocytes express toll-like receptors for bacterial products. *Glia* 43: 281–291

Campanelli JT, Sandrock RW, Wheatley W, Xue H, Zheng J, Liang F, Chesnut JD, Zhan M, Rao MS, Liu Y (2008) Expression profiling of human glial precursors. *BMC Dev Biol* 8: 102

Chomyk AM, Volsko C, Tripathi A, Deckard SA, Trapp BD, Fox RJ, Dutta R (2017) DNA methylation in demyelinated multiple sclerosis hippocampus. *Sci Rep* 7: 8696

Choudhry H, Harris AL (2018) Advances in hypoxia-inducible factor biology. *Cell Metab* 27: 281–298

Claudel M, Jouzeau JY, Cailotto F (2019) Secreted Frizzled-related proteins (sFRPs) in osteo-articular diseases: much more than simple antagonists of Wnt signaling? *FEBS J* 286: 4832–4851

Colonna M, Butovsky O (2017) Microglia function in the central nervous system during health and neurodegeneration. *Annu Rev Immunol* 35: 441–468

Constantinescu CS, Farooqi N, O'Brien K, Gran B (2011) Experimental autoimmune encephalomyelitis (EAE) as a model for multiple sclerosis (MS). *Br J Pharmacol* 164: 1079–1106

Dahl E, Wiesmann F, Woenckhaus M, Stoehr R, Wild PJ, Veeck J, Knüchel R, Klopocki E, Sauter G, Simon R *et al* (2007) Frequent loss of SFRP1 expression in multiple human solid tumours: association with aberrant promoter methylation in renal cell carcinoma. *Oncogene* 26: 5680–5691

Escartin C, Galea E, Lakatos A, O'Callaghan JP, Petzold GC, Serrano-Pozo A, Steinhäuser C, Volterra A, Carmignoto G, Agarwal A *et al* (2021) Reactive astrocyte nomenclature, definitions, and future directions. *Nat Neurosci* 24: 312–325

Escartin C, Guillemaud O, Carrillo-de Sauvage MA (2019) Questions and (some) answers on reactive astrocytes. *Glia* 67: 2221–2247

Esteve P, Bovolenta P (2010) The advantages and disadvantages of sfrp1 and sfrp2 expression in pathological events. *Tohoku J Exp Med* 221: 11–17

Esteve P, Crespo I, Kaimakis P, Sandonis A, Bovolenta P (2019a) Sfrp1 modulates cell-signaling events underlying telencephalic patterning, growth and differentiation. *Cereb Cortex* 29: 1059–1074

Esteve P, Rueda-Carrasco J, Inés Mateo M, Martin-Bermejo MJ, Draffin J, Pereyra G, Sandonís Á, Crespo I, Moreno I, Aso E *et al* (2019b) Elevated levels of Secreted-Frizzled-Related-Protein 1 contribute to Alzheimer's disease pathogenesis. *Nat Neurosci* 22: 1258–1268

Esteve P, Sandonìs A, Cardozo M, Malapeira J, Ibañez C, Crespo I, Marcos S, Gonzalez-Garcia S, Toribio ML, Arribas J *et al* (2011a) SFRPs act as negative modulators of ADAM10 to regulate retinal neurogenesis. *Nat Neurosci* 14: 562–569

Esteve P, Sandonis A, Ibanez C, Shimono A, Guerrero I, Bovolenta P (2011b) Secreted frizzled-related proteins are required for Wnt/beta-catenin signalling activation in the vertebrate optic cup. *Development* 138: 4179–4184

Folke J, Pakkenberg B, Brudek T (2019) Impaired Wnt signaling in the prefrontal cortex of Alzheimer's Disease. *Mol Neurobiol* 56: 873–891

Frank-Cannon TC, Alto LT, McAlpine FE, Tansey MG (2009) Does neuroinflammation fan the flame in neurodegenerative diseases? *Mol Neurodegener* 4: 47

García-Velázquez L, Arias C (2021) Differential regulation of Wnt signaling components during hippocampal reorganization after entorhinal cortex lesion. *Cell Mol Neurobiol* 41: 537–549

Glass CK, Saijo K, Winner B, Marchetto MC, Gage FH (2010) Mechanisms underlying inflammation in neurodegeneration. *Cell* 140: 918–934

Grassivaro F, Menon R, Acquaviva M, Ottoboni L, Ruffini F, Bergamaschi A, Muzio L, Farina C, Martino G (2020) Convergence between microglia and peripheral macrophages phenotype during development and neuroinflammation. *J Neurosci* 40: 784–795

Greter M, Lelios I, Croxford AL (2015) Microglia versus myeloid cell nomenclature during brain inflammation. *Front Immunol* 6: 249

Gunner G, Cheadle L, Johnson KM, Ayata P, Badimon A, Mondo E, Nagy MA, Liu L, Bemiller SM, Kim K-W *et al* (2019) Sensory lesioning induces microglial synapse elimination via ADAM10 and fractalkine signaling. *Nat Neurosci* 22: 1075–1088

Halleskog C, Schulte G (2013) WNT-3A and WNT-5A counteract lipopolysaccharide-induced pro-inflammatory changes in mouse primary microglia. *J Neurochem* 125: 803–808

Heinz S, Benner C, Spann N, Bertolino E, Lin YC, Laslo P, Cheng JX, Murre C, Singh H, Glass CK (2010) Simple combinations of lineage-determining transcription factors prime cis-regulatory elements required for macrophage and B cell identities. *Mol Cell* 38: 576–589

Helton R, Cui J, Scheel JR, Ellison JA, Ames C, Gibson C, Blouw B, Ouyang L, Dragatsis I, Zeitlin S *et al* (2005) Brain-specific knock-out of hypoxia-inducible factor-1alpha reduces rather than increases hypoxic-ischemic damage. *J Neurosci* 25: 4099–4107

Heneka MT, Kummer MP, Latz E (2014) Innate immune activation in neurodegenerative disease. *Nat Rev Immunol* 14: 463–477

Heppner FL, Greter M, Marino D, Falsig J, Raivich G, Hövelmeyer N, Waisman A, Rülicke T, Prinz M, Priller J *et al* (2005) Experimental autoimmune encephalomyelitis repressed by microglial paralysis. *Nat Med* 11: 146–152

Hickman S, Izzy S, Sen P, Morsett L, El Khoury J (2018) Microglia in neurodegeneration. *Nat Neurosci* 21: 1359–1369

Holm TH, Draeby D, Owens T (2012) Microglia are required for astroglial Toll-like receptor 4 response and for optimal TLR2 and TLR3 response. *Glia* 60: 630–638

Honarpisheh P, Lee J, Banerjee A, Blasco-Conesa MP, Honarpisheh P, d'Aigle J, Mamun AA, Ritzel RM, Chauhan A, Ganesh BP *et al* (2020) Potential caveats of putative microglia-specific markers for assessment of age-related cerebrovascular neuroinflammation. *J Neuroinflammation* 17: 366

Huang S, Choi MH, Huang H, Wang X, Chang YC, Kim JY (2020) Demyelination regulates the circadian transcription factor BMAL1 to signal adult neural stem cells to initiate oligodendrogenesis. *Cell Rep* 33: 108394

Hundhausen C, Schulte A, Schulz B, Andrzejewski MG, Schwarz N, von Hundelshausen P, Winter U, Paliga K, Reiss K, Saftig P *et al* (2007) Regulated shedding of transmembrane chemokines by the disintegrin and metalloproteinase 10 facilitates detachment of adherent leukocytes. *J Immunol* 178: 8064–8072

Ising C, Venegas C, Zhang S, Scheiblich H, Schmidt SV, Vieira-Saecker A, Schwartz S, Albasset S, McManus RM, Tejera D *et al* (2019) NLRP3 inflammasome activation drives tau pathology. *Nature* 575: 669–673

Jha MK, Jo M, Kim JH, Suk K (2019) Microglia-astrocyte crosstalk: an intimate molecular conversation. *Neuroscientist* 25: 227–240

Johnson ECB, Carter EK, Dammer EB, Duong DM, Gerasimov ES, Liu Y, Liu J, Betarbet R, Ping L, Yin L *et al* (2021) Large-Scale deep multi-layer analysis of Alzheimer's disease brain reveals strong proteomic disease-related changes not observed at the RNA level systems biology. *bioRxiv* https://doi.org/10.1101/2021.04.05.438450 [PREPRINT]

Jung S, Aliberti J, Graemmel P, Sunshine MJ, Kreutzberg GW, Sher A, Littman DR (2000) Analysis of fractalkine receptor CX(3)CR1 function by targeted deletion and green fluorescent protein reporter gene insertion. *Mol Cell Biol* 20: 4106–4114

Kaltschmidt B, Kaltschmidt C (2009) NF-kappaB in the nervous system. *Cold Spring Harb Perspect Biol* 1: a001271

Kapellos TS, Taylor L, Lee H, Cowley SA, James WS, Iqbal AJ, Greaves DR (2016) A novel real time imaging platform to quantify macrophage phagocytosis. *Biochem Pharmacol* 116: 107–119

Keller D, Erö C, Markram H (2018) Cell densities in the mouse brain: a systematic review. *Front Neuroanat* 12: 83

Keren-Shaul H, Spinrad A, Weiner A, Matcovitch-Natan O, Dvir-Szternfeld R, Ulland TK, David E, Baruch K, Lara-Astaiso D, Toth B *et al* (2017) A unique microglia type associated with restricting development of Alzheimer's disease. *Cell* 169: 1276–1290.e17

Kierdorf K, Prinz M (2013) Factors regulating microglia activation. *Front Cell Neurosci* 7: 44

Kim D, Paggi JM, Park C, Bennett C, Salzberg SL (2019) Graph-based genome alignment and genotyping with HISAT2 and HISAT-genotype. *Nat Biotechnol* 37: 907–915

Kleinberger G, Yamanishi Y, Suarez-Calvet M, Czirr E, Lohmann E, Cuyvers E, Struyfs H, Pettkus N, Wenninger-Weinzierl A, Mazaheri F *et al* (2014) TREM2 mutations implicated in neurodegeneration impair cell surface transport and phagocytosis. *Sci Transl Med* 6: 243ra86

Kuhn PH, Wang H, Dislich B, Colombo A, Zeitschel U, Ellwart JW, Kremmer E, Rossner S, Lichtenthaler SF (2010) ADAM10 is the physiologically relevant, constitutive alpha-secretase of the amyloid precursor protein in primary neurons. *EMBO J* 29: 3020–3032

Kunkle BW, Grenier-Boley B, Sims R, Bis JC, Damotte V, Naj AC, Boland A, Vronskaya M, van der Lee SJ, Amlie-Wolf A *et al* (2019) Genetic meta-analysis of diagnosed Alzheimer's disease identifies new risk loci and implicates Abeta, tau, immunity and lipid processing. *Nat Genet* 51: 414–430

Lee YS, Lee KA, Yoon HB, Yoo SA, Park YW, Chung Y, Kim WU, Kang CY (2012) The Wnt inhibitor secreted Frizzled-Related Protein 1 (sFRP1) promotes human Th17 differentiation. *Eur J Immunol* 42: 2564–2573

Li H, Handsaker B, Wysoker A, Fennell T, Ruan J, Homer N, Marth G, Abecasis G, Durbin R, 1000 Genome Project Data Processing Subgroup (2009) The sequence Alignment/Map format and SAMtools. *Bioinformatics* 25: 2078–2079

Lichtenthaler SF, Lemberg MK, Fluhrer R (2018) Proteolytic ectodomain shedding of membrane proteins in mammals-hardware, concepts, and recent developments. *EMBO J* 37: e99456

Love MI, Huber W, Anders S (2014) Moderated estimation of fold change and dispersion for RNA-seq data with DESeq2. *Genome Biol* 15: 550

Marin V, Stornaiuolo A, Piovan C, Corna S, Bossi S, Pema M, Giuliani E, Scavullo C, Zucchelli E, Bordignon C *et al* (2016) RD-MolPack technology for the constitutive production of self-inactivating lentiviral vectors pseudotyped with the nontoxic RD114-TR envelope. *Mol Ther Methods Clin Dev* 3: 16033

Marinelli S, Basilico B, Marrone MC, Ragozzino D (2019) Microglia-neuron crosstalk: signaling mechanism and control of synaptic transmission. *Semin Cell Dev Biol* 94: 138–151

Martin-Manso G, Calzada MJ, Chuman Y, Sipes JM, Xavier CP, Wolf V, Kuznetsova SA, Rubin JS, Roberts DD (2011) sFRP-1 binds via its netrin-related motif to the N-module of thrombospondin-1 and blocks

thrombospondin-1 stimulation of MDA-MB-231 breast carcinoma cell adhesion and migration. *Arch Biochem Biophys* 509: 147−156

Mazaheri F, Snaidero N, Kleinberger G, Madore C, Daria A, Werner G, Krasemann S, Capell A, Trumbach D, Wurst W *et al* (2017) TREM2 deficiency impairs chemotaxis and microglial responses to neuronal injury. *EMBO Rep* 18: 1186−1198

Merten OW, Hebben M, Bovolenta C (2016) Production of lentiviral vectors. *Mol Ther Methods Clin Dev* 3: 16017

Mii Y, Taira M (2009) Secreted Frizzled-related proteins enhance the diffusion of Wnt ligands and expand their signalling range. *Development* 136: 4083−4088

Musardo S, Marcello E, Gardoni F, Di Luca M (2014) ADAM10 in synaptic physiology and pathology. *Neurodegener Dis* 13: 72−74

Palomer E, Buechler J, Salinas PC (2019) Wnt signaling deregulation in the aging and Alzheimer's brain. *Front Cell Neurosci* 13: 227

Perry VH, Holmes C (2014) Microglial priming in neurodegenerative disease. *Nat Rev Neurol* 10: 217−224

Piccio L, Buonsanti C, Mariani M, Cella M, Gilfillan S, Cross AH, Colonna M, Panina-Bordignon P (2007) Blockade of TREM-2 exacerbates experimental autoimmune encephalomyelitis. *Eur J Immunol* 37: 1290−1301

Prox J, Bernreuther C, Altmeppen H, Grendel J, Glatzel M, D'Hooge R, Stroobants S, Ahmed T, Balschun D, Willem M *et al* (2013) Postnatal disruption of the disintegrin/metalloproteinase ADAM10 in brain causes epileptic seizures, learning deficits, altered spine morphology, and defective synaptic functions. *J Neurosci* 33: 12915−12928

Ransohoff RM (2016) How neuroinflammation contributes to neurodegeneration. *Science* 353: 777−783

Ransohoff RM, Perry VH (2009) Microglial physiology: unique stimuli, specialized responses. *Annu Rev Immunol* 27: 119−145

Rivest S (2009) Regulation of innate immune responses in the brain. *Nat Rev Immunol* 9: 429−439

Rolls A, Shechter R, London A, Ziv Y, Ronen A, Levy R, Schwartz M (2007) Toll-like receptors modulate adult hippocampal neurogenesis. *Nat Cell Biol* 9: 1081−1088

Saftig P, Lichtenthaler SF (2015) The alpha secretase ADAM10: a metalloprotease with multiple functions in the brain. *Prog Neurogibol* 135: 1−20

Sarlus H, Heneka MT (2017) Microglia in Alzheimer's disease. *J Clin Invest* 127: 3240−3249

Satoh W, Gotoh T, Tsunematsu Y, Aizawa S, Shimono A (2006) Sfrp1 and Sfrp2 regulate anteroposterior axis elongation and somite segmentation during mouse embryogenesis. *Development* 133: 989−999

Sole-Domenech S, Cruz DL, Capetillo-Zarate E, Maxfield FR (2016) The endocytic pathway in microglia during health, aging and Alzheimer's disease. *Ageing Res Rev* 32: 89−103

Suh J, Choi SH, Romano DM, Gannon MA, Lesinski AN, Kim DY, Tanzi RE (2013) ADAM10 missense mutations potentiate beta-amyloid accumulation by impairing prodomain chaperone function. *Neuron* 80: 385−401

Thorvaldsdottir H, Robinson JT, Mesirov JP (2013) Integrative Genomics Viewer (IGV): high-performance genomics data visualization and exploration. *Brief Bioinform* 14: 178−192

Trevant B, Gaur T, Hussain S, Symons J, Komm BS, Bodine PV, Stein GS, Lian JB (2008) Expression of secreted frizzled related protein 1, a Wnt antagonist, in brain, kidney, and skeleton is dispensable for normal embryonic development. *J Cell Physiol* 217: 113−126

Turnbull IR, Gilfillan S, Cella M, Aoshi T, Miller M, Piccio L, Hernandez M, Colonna M (2006) Cutting edge: TREM-2 attenuates macrophage activation. *J Immunol* 177: 3520−3524

Ulland TK, Song WM, Huang S-C, Ulrich JD, Sergushichev A, Beatty WL, Loboda AA, Zhou Y, Cairns NJ, Kambal A *et al* (2017) TREM2 maintains microglial metabolic fitness in Alzheimer's disease. *Cell* 170: 649−663.e13

Van Steenwinckel J, Schang AL, Krishnan ML, Degos V, Delahaye-Duriez A, Bokobza C, Csaba Z, Verdonk F, Montane A, Sigaut S *et al* (2019) Decreased microglial Wnt/beta-catenin signalling drives microglial pro-inflammatory activation in the developing brain. *Brain* 142: 3806−3833

Wang W-H, McNatt LG, Pang I-H, Millar JC, Hellberg PE, Hellberg MH, Steely HT, Rubin JS, Fingert JH, Sheffield VC *et al* (2008) Increased expression of the WNT antagonist sFRP-1 in glaucoma elevates intraocular pressure. *J Clin Invest* 118: 1056−1064

Wendelen A-C, Degenhardt K, Kaurani L, Gertig M, Ulas T, Jain G, Wagner J, Häsler LM, Wild K, Skodras A *et al* (2018) Innate immune memory in the brain shapes neurological disease hallmarks. *Nature* 556: 332−338

Wheeler MA, Jaronen M, Covacu R, Zandee SEJ, Scalisi G, Rothhammer V, Tjon EC, Chao C-C, Kenison JE, Blain M *et al* (2019) Environmental control of astrocyte pathogenic activities in CNS inflammation. *Cell* 176: 581−596.e18

Wong KK, Zhu F, Khatri I, Huo Q, Spaner DE, Gorczynski RM (2016) Characterization of CD200 ectodomain shedding. *PLoS One* 11: e0152073

Wright GJ, Puklavec MJ, Willis AC, Hoek RM, Sedgwick JD, Brown MH, Barclay AN (2000) Lymphoid/neuronal cell surface OX2 glycoprotein recognizes a novel receptor on macrophages implicated in the control of their function. *Immunity* 13: 233−242

Wright SD (1999) Toll, a new piece in the puzzle of innate immunity. *J Exp Med* 189: 605−609

Youm Y-H, Grant R, McCabe L, Albarado D, Nguyen K, Ravussin A, Pistell P, Newman S, Carter R, Laque A *et al* (2013) Canonical Nlrp3 inflammasome links systemic low-grade inflammation to functional decline in aging. *Cell Metab* 18: 519−532

Yu G, Wang LG, Han Y, He QY (2012) clusterProfiler: an R package for comparing biological themes among gene clusters. *OMICS* 16: 284−287

Zhang YE, Sloan S, Clarke L, Caneda C, Plaza C, Blumenthal P, Vogel H, Steinberg G, Edwards M, Li G *et al* (2016) Purification and characterization of progenitor and mature human astrocytes reveals transcriptional and functional differences with mouse. *Neuron* 89: 37−53